# Towards a Better Understanding of the Magnetic Interactions within *m*-Phenylene $\alpha$-Nitronyl Imino Nitroxide Based Biradicals

**Laure Catala,[a] Jacques Le Moigne,[b] Nathalie Kyritsakas,[c] Paul Rey,[d] Juan J. Novoa,[e] and Philippe Turek*[a]**

**Abstract:** An extensive investigation of the magnetic properties of three series of biradicals (bis-nitronyl nitroxides **diNN-R**, bis-imino nitroxides **diIN-R** and mixed **INNN-R**, where R is either hydrogen, a triple bond or trimethylsilylacetylenic group) has been carried out to give clear values of the intramolecular interactions through the *m*-phenylene coupling unit with $\alpha$-nitronyl nitroxides (**NN**) or $\alpha$-imino nitroxides (**IN**). An EPR study of the molecules in the isolated state is validated by ab initio calculations, which show the respective influence of spin polarisation and molecular conformation on the singlet–triplet gaps. All these results indicate that the triplet state is the ground state for such biradicals, except when the imidazolyl cycles are orthogonal to the phenyl ring. The magnetic properties of the biradicals in the solid state can be rationalised by examination of the short contacts produced between the ONCNO and ONCN groups. EPR studies on single crystals of the H-substituted series have confirmed the presence of a structural distortion for **diNN-H** whereas **diIN-H** and **INNN-H** do not exhibit such a peculiarity. The magnetic behaviour of **diIN-H** is described well by a four-spins model, with a strong intermolecular antiferromagnetic interaction of $-90$ K, whereas in the case of the two other compounds, a supplementary contact involves more complex interactions between the dimers. The compound **diNN-tmsa** exhibits a ferromagnetic intermolecular interaction of $+11$ K within the dimers, and this could be attributed to the relative disposition of the imidazolyl rings. Compound **diNN-tr** reveals a chain-like behaviour, whereas **diIN-tr** shows a predominant antiferromagnetic interaction within the dimers. The values for the intramolecular interactions in the solid state are in good agreement with those found for the isolated molecules.

**Keywords:** biradicals · magnetic properties · molecular devices · $\alpha$-nitronyl nitroxide · triplet ground state

## Introduction

Much interest has been devoted to the $\alpha$-nitronyl nitroxide (**NN**) radical derivatives in the field of organic molecular magnetism,[1] since the discovery of the first purely organic ferromagnet.[2] **NN** radical derivatives afford a versatile chemistry provided that they are fairly stable in air at room temperature. Numerous derivatives have been synthesised which exhibit a large variety of magnetic behaviours.[3] In addition to the production of a range of competitive Curie temperatures, the challenge with these materials is to achieve a better understanding of the magnetic interactions within assemblies of so-called open-shell molecules. These interactions can be either *intra*molecular, when more than one radical is connected through a chemical coupler, or *inter*molecular, when an assembly of molecules is considered. The former strategy consists of the use of a conjugated coupler, which provides a definite sign of the exchange interaction by a controlled connectivity of the paramagnetic fragments, and hence results in a high-spin molecule. Different models have been proposed to describe and predict the ground states of

[a] Prof. P. Turek, Dr. L. Catala
Institut Charles Sadron, 6, rue Boussingault
CNRS, 67083 Strasbourg (France)
Fax: (+33) 3-88-41-40-99
E-mail: turek@ics.u-strasbg.fr

[b] Dr. J. Le Moigne
Institut de Physique et Chimie des Matériaux de Strasbourg
UMR 7504, 23, rue du Loess, 67037 Strasbourg (France)

[c] Dr. N. Kyritsakas
Laboratoire de Cristallochimie et Chimie Structurale associé au CNRS
Université Louis Pasteur
Institut Le Bel, 4, rue Blaise Pascal, 67000 Strasbourg (France)

[d] Dr. P. Rey
CEA-Grenoble, DRFMC/SCIB/CC, 17, rue des Martyrs
38054 Grenoble Cedex 9 (France)

[e] Prof. J. J. Novoa
Departament de Quimica Fisica
Facultat de Fisica i Quimica
Universitat de Barcelona, 08028, Barcelona (Spain)

Supporting information for this article is available on the WWW under http://www.wiley-vch.de/home/chemistry/ or from the author

  0947-6539/01/0711-2466 $ 17.50+.50/0 *Chem. Eur. J.* **2001**, *7*, No. 11

non-Kekule hydrocarbons.[4] These rules can serve as a basis for the design of high-spin molecules, but they cannot be extended a priori to hetero-atom-containing radicals and couplers. Furthermore, it has been shown that the conformation plays a decisive role in the spin multiplicity of the ground state.[5] The experimental and/or theoretical study of the intramolecular magnetic interactions is thus necessary for each coupler/radical system prior to its use in a larger assembly within a given synthetic strategy.[6]

The intermolecular strategy is based on using supramolecular engineering tools such as hydrogen bonds or $\pi-\pi$ stacking in order to give a better predictability of the structural arrangements.[7] Some examples actually illustrate the use of these tools,[3b,e, 8] and some results show unequivocally that the hydrogen bond is able to transmit magnetic exchange.[3e, 8j] It is obviously necessary to control the molecular packing within molecular materials designed for use as molecular magnets, since magnetism is a cooperative phenomenon. However, it has been shown recently that there are no relevant rules for the magnetic properties to structure relationships, the so-called magneto-structural correlations, to understand the magnetic behaviour of the known molecular magnets.[9] It is still not possible to get a correct prediction of the intramolecular/intermolecular magnetic properties of an isolated molecule/bulk material by examination of the chemical connectivity/crystal structure only. Some step by step methodologies have been developed for both strategies, in order to obtain a better understanding of these complex phenomena.

We have previously reported the lack of ferromagnetic coupling within a series of $\alpha$-imino nitroxide (**IN**) biradicals connected through a phenylethynyl coupler.[10] The target of the present work was to study this coupler connecting potential spin entities $S=1$ instead of spin $S=½$. The triplet spins were designed by coupling together **IN** and/or **NN** radicals through the *m*-phenylene unit. This connectivity is known to yield a ferromagnetic coupling within such biradicals, although some contradictory results have been reported.[11] Therefore, before the design of complex oligoradicals based on such $S=1$ biradicals could be achieved, it was essential to have a precise understanding of the magnetic behaviour of the basic $S=1$ building block.

We report on the magnetic properties of a series of biradicals based on a substituted phenyl connected in the *meta* position **IN** and/or **NN** radicals. In the first part, the ground state of these biradicals as well as the strength of the intramolecular magnetic exchange interactions is properly assessed with EPR experiments and ab initio calculations

**Abstract in French:** *Une étude approfondie des propriétés magnétiques a été menée sur trois séries biradicalaires (bis-nitronyl nitroxydes* ***diNN-R****, bis-imino nitroxydes* ***diIN-R*** *et mixte* ***INNN-R****, oû R désigne soit un atome d'hydrogène, une liaison triple ou un groupe triméthylsilylacetyléne), afin de déterminer avec précision les valeurs des interactions intramoléculaires à travers l'unité m-phénylène porteuse de radicaux de type α-nitronyl nitroxyde et α-imino nitroxyde. L'étude des molécules à l'état isolé par la technique de RPE a été validée par des calculs ab initio, qui ont démontré l'influence respective de la polarisation de spin et de la conformation moléculaire sur les valeurs de l'écart singulet–triplet. L'ensemble de ces résultats a mis en évidence un état fondamental triplet pour tous les biradicaux, excepté lorsque les cycles imidazolyles sont orthogonaux au cycle phényle. Les propriétés à l'état solide ont pu être explicitées par des corrélations magnéto-structurales basées sur la considération de contacts courts entre les groupes ONCNO ou ONCN. Des études RPE sur des monocristaux orientés de la série de biradicaux non-substitués ont confirmé la présence d'une distorsion structurale à 30 K dans le cas du composé* ***diNN-H****, tandis que les composés* ***INNN-H*** *et* ***diIN-H*** *ne présentent pas cette particularité. Le comportement du composé* ***diIN-H*** *a pu être correctement décrit par un modèle de 4 spins, avec une forte interaction intermoléculaire antiferromagnétique de −90 K. Le composé* ***diNN-tmsa*** *présente une interaction ferromagnétique de +11 K au sein de dimères, liée à la disposition relative des cycles imidazolyle. Un chemin d'échange au sein de chaînes alternées a été mis en évidence pour le composé* ***diNN-tr****, tandis que le composé* ***diIN-tr*** *présente une interaction antiferromagnétique dominante au sein de dimères en tête-bêche. Les valeurs trouvées lors des modélisations des interactions intramoléculaires à l'état solide sont en accord avec celles obtenues lors des études expérimentales à l'état isolé.*

**Abstract in Spanish:** *Se ha llevado a cabo una investigación exhaustiva de las propiedades magnéticas de tres series de biradicales (bis-nitronil nitróxidos* ***diNN-R****, imino nitróxidos* ***diIN-R****, mixto* ***INNN-R****, con R = hydrogeno, enlace triple o grupo trimetilsililacetilenico), a fin clarificar la naturaleza y magnitud de las interacciones magnéticas intramoleculares que se producen entre nitronil nitróxidos o imino nitróxidos a través de la unidad acopladora m-fenileno. El estudio EPR de las moleculas aisladas se ha validado mediante cálculos ab initio que muestran la influencia de la polarización de spin y la conformación en las separaciones singlete-triplete. Los resultados indican que, salvo cuando los anillos de imidazolil son ortogonales al anillo fenílico, el estado fundamental de estos biradicales es el triplete. Las propiedades magnéticas de los sólidos pueden racionalizarse mirando los contactos cortos que se producen entre los grupos ONCNO o ONCN. Estudios EPR sobre monocristales de los compuestos de la serie de biradicales H sustituidos confirman la presecia de una distorsión estructural dentro del* ***diNN-H****, que no existe en el* ***diIN-H*** *o* ***INNN-H****. El comportamiento magnético del* ***diIN-H*** *está bién descrito mediante un modelo de cuatro spines, con una interacción intermolecular fuerte de −90 K, mientras que para los otros dos compuestos un contacto suplementario da lugar a interacciones más complejas entre los dímeros. El compuesto* ***diNN-tmsa*** *presenta entre los dímeros una interacción ferromagnética de +11 K, que puede atribuirse a la disposición relativa de los anillos de imidazolil. Por otra parte,* ***diNN-tr*** *se comporta como una cadena, mientras que* ***diIN-tr*** *presenta una interacción predominante antiferromagnética entre sus dímeros. Los valores encontrados para las interacciones intramoleculares en estado sólido son semejantes a los encontrados para las moleculas aisladas.*

  0947-6539/01/0711-2467 $ 17.50+.50/0 

performed in the isolated state. Furthermore, such very close molecules differing chemically in the substituent on the phenyl ring, give isostructural compounds in the crystalline state. Indeed, replacing **NN** by **IN** only suppresses one oxygen atom within the radical moiety. Within such a coherent series the growth of single crystals was successful. Slight modifications of some intermolecular contacts result in different magnetic properties of the bulk materials. The second part of this paper is thus devoted to the description of the used methodology. Relevant conclusions on the magneto–structural correlations within the different series were therefore drawn.

## Results and Discussion

**Preparation of biradicals**: Routes to biradicals **diNN-R**, **INNN-R** and **diIN-R** are summarised in Scheme 1. After a four-step synthesis, the 5-bromoisophthalaldehyde was obtained,[12] then transformed into 5-trimethylsilylacetylene isophthalaldehyde by Sonogashira's coupling[13] and deprotected by $K_2CO_3$ in methanol to give the 5-ethynylisophthalaldehyde. The diformyl derivatives were treated with bishydroxylamine[14] in a procedure which afforded high yields of pure precursors, and the desired **NN**-based biradicals were obtained after standard oxidation procedure with $NaIO_4$ in a dichloromethane/water mixture.[15] The deoxygenation of one or two **NN** radicals of **diNN-R** compounds to give the **INNN-R** and **diIN-R** compounds was achieved by addition of $NaNO_2$ (2 and 10 equivalents, respectively, following the reaction by TLC), in an acidified dichloromethane/water mixture. Single crystals were obtained for all compounds (except for **diIN-tmsa** and **INNN-tr**) by slow evaporation or diffusion in a dichloromethane/hexane mixture.

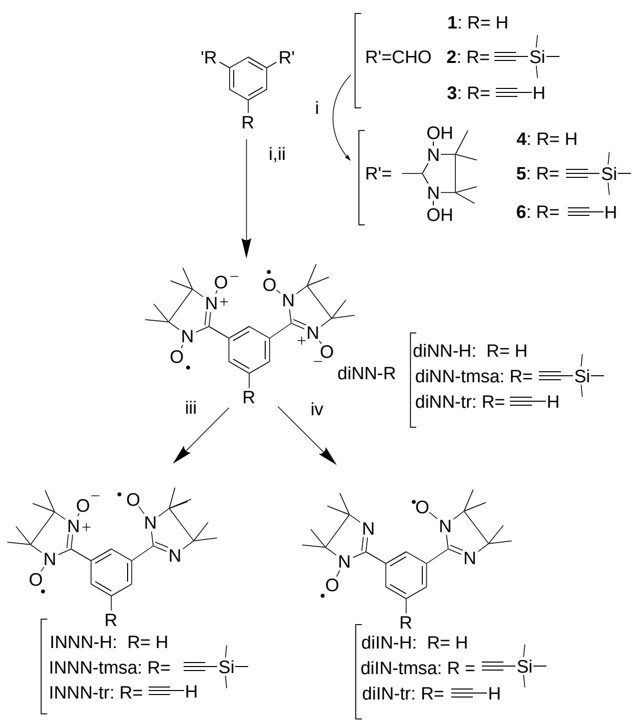


Scheme 1. i) 2,3-Bishydroxylamine dimethylbutane, MeOH, Ar; ii) $NaIO_4$; iii) 10 equiv $NaNO_2$; iv) 2 equiv $NaNO_2$.

**Intramolecular magnetic properties**: The EPR spectra of the **diNN-R** series in fluid solutions are best resolved in dilute acetone solutions (Figure 1a). The individual components of the expected nine-line pattern are broadened by dipolar through-space interactions, owing to the through-space proximity of the radicals. Assuming the strong exchange limit, that is, the exchange interaction between radical fragments, $J$ is much larger than the hyperfine coupling constant (hfcc).[16] The experimental spectra are reproduced well with the hfcc for the four equivalent $^{14}N$ nuclei, $a_N = 3.70$ G, with the average $g$ value, $g = 2.0067$, and a Lorentzian/Gaussian ratio, $r = 0.5$, for the lineshape of the individual components of peak-to-peak linewidth, $\Delta B_{pp} = 3$ G. The EPR spectrum of the **INNN-R** compounds exhibit a poorly resolved eight-line spectrum in acetone (Figure 1b). This spectrum can be reproduced assuming the strong exchange limit within a set of four interacting $^{14}N$ nuclei, with two equivalent $^{14}N$ nuclei within the **NN** fragment with $a_N = 3.75$ G, and the **IN** radical

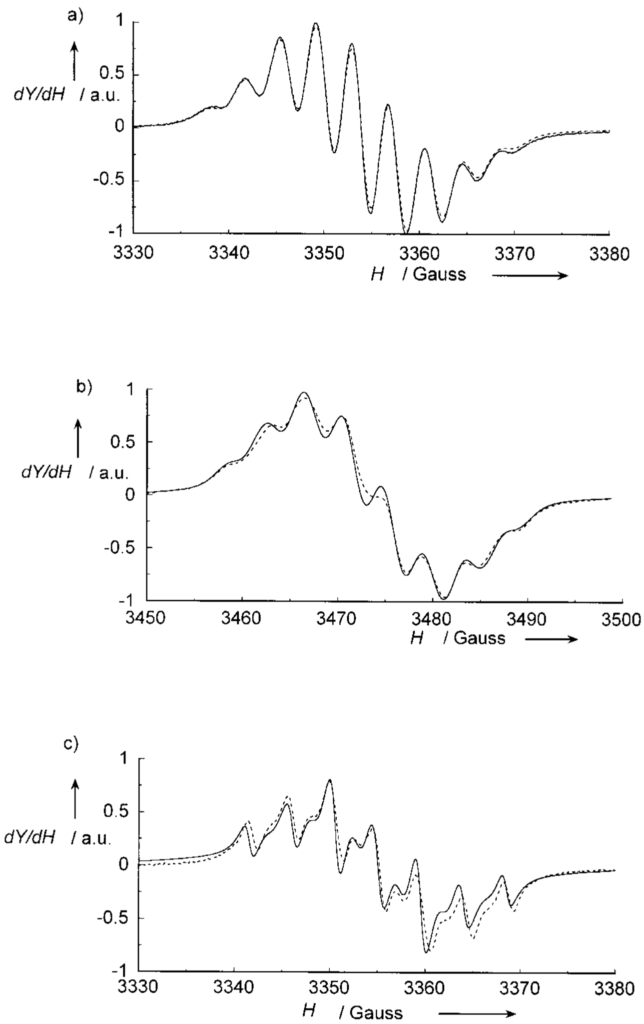


Figure 1. EPR spectra and simulations (dotted line) of diluted ($10^{-4}$ M) biradicals in acetone: a) **diNN-tr**; b) **INNN-H**; c) **diIN-H**.



0947-6539/01/0711-2468 $ 17.50+.50/0 *Chem. Eur. J.* **2001**, *7*, No. 11

fragment with two unequivalent nuclei with $a_{N1} = 4.5$ G, and $a_{N2} = 2.2$ G ($\Delta B_{pp} = 3$ G, $r = 0.5$). The **diIN-R** solutions (Figure 1c) are reproduced reasonably well assuming the overlap of: i) a bis-imino nitroxide biradical within the strong exchange limit with $a_{N1} = 4.50$ G, $a_{N2} = 2.23$ G ($\Delta B_{pp} = 2.2$ G, $g = 2.0061$); ii) a fraction of a purely dipolar component (gaussian, $\Delta B = 12$ G, for example, 10% within the **diIN-H** compound in Figure 1c); and iii) a fraction of uncoupled biradical, for example, 10% monoradical for the **diIN-H** compound with $a_{N1} = 9$ G, $a_{N2} = 4.5$ G ($\Delta B_{pp} = 2.2$ G, $g = 2.0061$). It is worth noticing that this type of biradical is very sensitive to the conformational modifications such as to nearly interrupt coupling between the radical entities, whereas only strong exchange was observed for the two other families of compounds.

The effect of conformation on intramolecular exchange is well illustrated by the EPR solution spectra obtained in THF. These are not affected in the case of **diNN-R** compounds. However, the decoupling of the radical fragments is clearly observed for the **diIN-R** and **INNN-R** compounds (Figure 2a,b). The spectrum of an **IN** monoradical is solely observed for the **diIN-R** derivatives (Figure 2a).

A satisfactory simulation of the solution spectra of the **INNN-R** derivatives (Figure 2b) is obtained assuming the overlap of the spectrum of: i) an **IN** monoradical ($a_{N1} = 9$ G, $a_{N2} = 4.5$ G, $\Delta B_{pp} = 1$ G, $g = 2.0061$); ii) an **NN** monoradical ($a_N = 7.3$ G, $\Delta B = 1$ G, $g = 2.0067$); and iii) 10% of a dipolar component with $\Delta B_{pp} = 12$ G. Therefore, it is suggested that THF has a peculiar solvation effect, and this effect gives rise to a larger twist of the **IN** ring with respect to the phenyl ring. The presence of a bulkier **NN** radical prevents this solvation effect. The present observations agree with the previously reported EPR spectra for **IN/NN** biradical series, which are not affected within the bulkier 2-MeTHF.[15]

The frozen solutions have been studied for the nonsubstituted series in a dichloromethane/xylene 1:1 mixture, and in a 2-MeTHF for **diNN-H** in order to compare the values with the reference data.[15] In order to access a larger temperature range for the studies, the dilution of the biradicals within a polystyrene matrix has also been carried out. All the EPR spectra exhibit fine structure components as expected for these biradicals. Moreover, a half-field signal ("forbidden" $\Delta M_S = \pm 2$ transition) is observed for all compounds, and thus demonstrates the biradical nature of these compounds. The zero-field splitting (ZFS) parameters are reported in Table 1

Table 1. Zero field splitting parameters estimated from the EPR spectra of the biradicals diluted into frozen solution or in polymer matrix. The observation of another molecular conformation and the corresponding parameters are marked by an asterisk. The total number of lines is reported as *N*.

| Compound | Type of matrix | *N* | $D'$/Gauss | $E'$/Gauss |
|---|---|---|---|---|
| **diNN-H** | MeTHF | 4 | $94 \pm 5$ | 4 |
| | xylene/$CH_2Cl_2$ | 4 | $98 \pm 5$ | 1 |
| | polystyrene | 4 | $105 \pm 5$ | 5 |
| **diIN-H** | xylene/$CH_2Cl_2$ | 4 | $90 \pm 2$ | 3 |
| | polystyrene | 6 | $90 \pm 2$, $58 \pm 2$* | 4 |
| **INNN-H** | xylene/$CH_2Cl_2$ | 4 | $67 \pm 4$ | 3 |
| | Polystyrene | 6 | $144 \pm 5$, $69 \pm 2$* | 2 |
| **diNN-tr** | xylene/$CH_2Cl_2$ | 4 | $111 \pm 5$ | 0 |
| **diIN-tr** | xylene/$CH_2Cl_2$ | 4 | $90 \pm 2$ | 4 |
| **diNN-tmsa** | xylene/$CH_2Cl_2$ | 4 | $111 \pm 5$ | 0 |

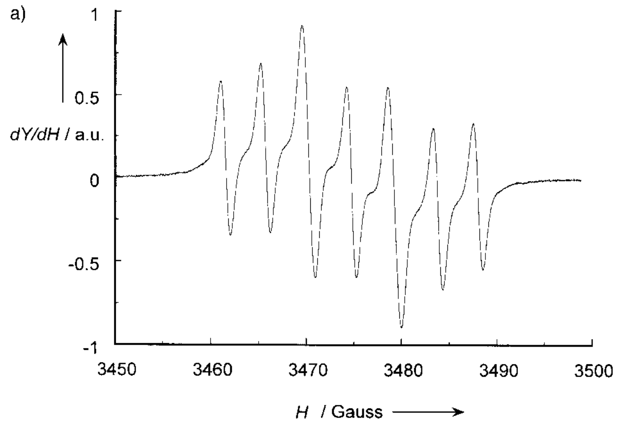


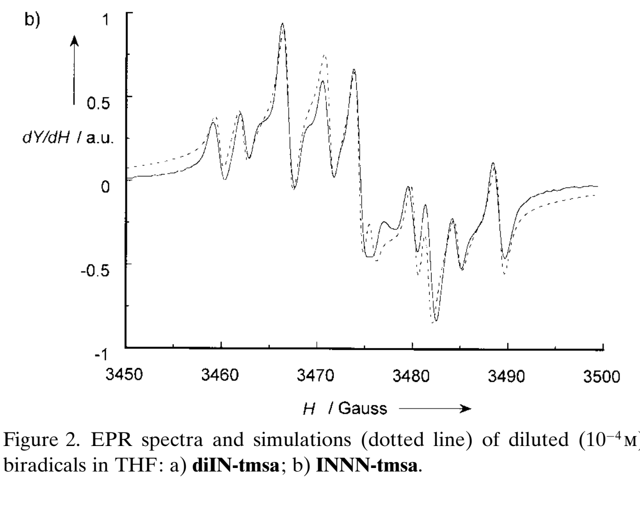


Figure 2. EPR spectra and simulations (dotted line) of diluted ($10^{-4}$ M) biradicals in THF: a) **diIN-tmsa**; b) **INNN-tmsa**.

in magnetic field units ($D'$,$E'$). In the case of **diNN-R**, the ZFS parameters are similar in a polystyrene matrix and in frozen solutions. Therefore, we may infer the same conformation within both media. Additional fine structure components are observed within the polystyrene matrix for the biradicals with one or two **IN** radicals. These are attributed to the two possible positions for the NO group, when flipping by 180° about the five-membered ring. From examination of the $D'$ values for compounds with different substituents R = H, tmsa, tr, it may be concluded that these do not strongly affect the overall conformation of the biradicals.

Interestingly, the $J$ values previously reported for **diNN-H** are in disagreement.[11] Alternatively, the singlet–triplet gap values assessed are $J/k_B > 100$ K,[11a] $J/k_B = 0$ K[11b] or $J/k_B = 23$ K, respectively.[11c] The last value is the best accepted estimation, since it reports on a state close to the isolated molecule. In the present work, this value has been checked, and the intramolecular exchange interaction has been assessed within the biradical derivatives from the careful recording of the temperature dependence of the EPR susceptibility, $\chi_{EPR}$, taking into account the difficulties discussed by various authors.[17] In most cases, the temperature dependence of the peak-to-peak amplitude, $A_{pp}$, of the half-field signal is representative of the evolution of $\chi_{EPR}$ versus temperature, since no signal distortion is observed throughout the studied temperature range. Moreover, a similar behaviour has been shown from the study of the integrated EPR susceptibility for both the $\Delta M_S = \pm 2$ and the $\Delta M_S = \pm 1$ absorption lines, as shown in Figure 3c. The data are fitted to

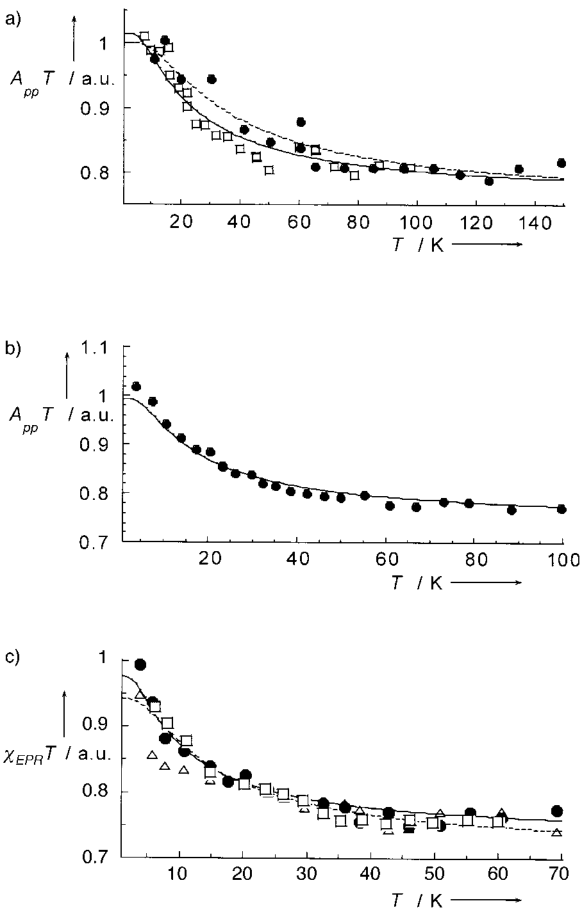


Figure 3. Temperature dependence of the EPR magnetic susceptibility ($\chi T$ product) determined with the use of various parameters (● peak-to-peak amplitude $A_{pp}T$ for the $\Delta M_s = \pm 1$ line, Δ peak-to-peak amplitude $A_{pp}T$ for the $\Delta M_s = \pm 2$ line; □ integrated intensity $\chi_{EPR}T$ for the $\Delta M_s = \pm 2$ line): a) **diNN-H** compound, **diNN-tr**; b) **INNN-H**; c) **diIN-H**.

the well-known Bleaney–Bowers law for two interacting $S = ½$ spins.[18] First of all, the triplet ground state is found for all compounds. This ascertains the transmission of ferromagnetic exchange coupling through the *m*-phenylene unit between the present **IN/NN** radical fragments. The values of the singlet–triplet (ST) gap is estimated as $J/k_B = 36 \pm 10$ K for **diNN-H** in a polystyrene matrix, $J/k_B = 23 \pm 5$ K for **diNN-tr** in a dichloromethane/xylene solution, $J/k_B = 19 \pm 6$ K for **INNN-H** and $J/k_B = 10 \pm 5$ K for **diIN-H** both in a polystyrene matrix. The S–T gap obtained for **diNN-R** is fairly close to the previously reported "best" estimation for the **diNN-H**.[11c]

A hierarchy is noticed for $J$ within the series of biradicals in the order $J$(**diIN-R**) < $J$(**INNN-R**) < $J$(**diNN-R**). However, the exchange interaction may be significantly affected by the molecular conformation as already discussed for the fluid solutions. In order to confirm the observed trend, ab initio calculations have been performed. These calculations allow the estimation of the respective roles of spin polarisation and conformation on the $J$ value, as reported below.

**Ab initio calculations**: The values of the computed S–T gaps are obtained by broken symmetry[19] density functional computations, using the B3LYP nonlocal exchange-correlation functional and the 3-21g* basis set (as implemented in Gaussian 98[20]). This approach has been used in other work aimed at computing the S–T gaps in dimers,[21] and its foundations have been largely discussed.[22] Before extending this approach to organic biradicals, we have tested its quality by checking that it reproduces the values and trends predicted by GVB-ROHF and CASSCF computations[23] on similar *m*-phenylene nitroxide (**1b**, R = HNO$^\bullet$) and methylene biradicals (**1c**, R = $CH_2^\bullet$). Our results, reported in Table 2 together

Table 2. Singlet–triplet gaps and spin density on the $C_2$ aromatic carbon for *m*-phenylene with two nitroxides (HNO$^\bullet$) or methylene ($CH_2^\bullet$) by B3LYP, GVB[23] or CASSCF[23] computations.

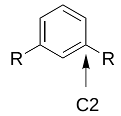


**1**

| Dihedral angle | R = HNO$^\bullet$ | | R = HNO$^\bullet$ | |
|---|---|---|---|---|
| | B3LYP/GVB[23] | $\rho_{C2}$ | B3LYP/GVB/CASSCF[23] | $\rho_{C2}$ |
| 0 | 617/141 | –0.151 | 3726/1384/5415 | –0.325 |
| 30 | 402/90 | –0.126 | 2572 | –0.313 |
| 60 | 67/15 | –0.063 | 381 | –0.254 |
| 90 | –15/–38 | –0.022 | –200/–130/–90 | –0.150 |

with the literature results, show the good qualitative agreement obtained. In addition, the S–T gap has been computed for the 1,3-bis(*tert*-butyl nitroxide)benzene (**1d**, R = *t*BuNO$^\bullet$) when a 30° dihedral angle is present between the phenyl and the NO groups. The broken symmetry B3LYP computed value of 240 K is found to be in good agreement with the reported experimental values for molecules based on this biradical.[24]

After establishing the reliability of the computational method, we performed calculations on the three compounds of interest, **diNN-H**, **INNN-H** and **diIN-H**. The molecular geometry of the molecules is that found in the crystal. The conformation of the three molecules is similar, with a dihedral angle between the five and six-membered rings close to 30°. In the **INNN-H** compound, we only studied the conformation in which the NO group of the **IN** fragment is placed pointing towards the **NN** group (that is, in an internal position $O_3$).

  0947-6539/01/0711-2470 $ 17.50+.50/0 

The results of these computations, reported in Table 3, show that the *triplet state* is the ground state in the three compounds at their crystal geometry. The computed S–T gaps are of the order of magnitude of the experimental values, with the hierarchy: **diNN-H** ($J/k_B = 94$ K) > **INNN-H** ($J/k_B = 38$ K) > **diIN-H** ($J/k_B = 11$ K). These values are proportional to the size of the spin polarisation found in these molecules, measured by the size of the atomic spin population on the $C_\alpha$ atom of the five-membered ring, larger in the **NN** than in the **IN** ring. This is also reflected by the spin density spread over the phenyl ring, and is even greater when the radicals connected are **NN** (see the atomic spin population, $\rho_{C2}$, borne by the C2 atom of the phenyl ring, that to which the five-membered rings are attached, reported in Table 3). However,

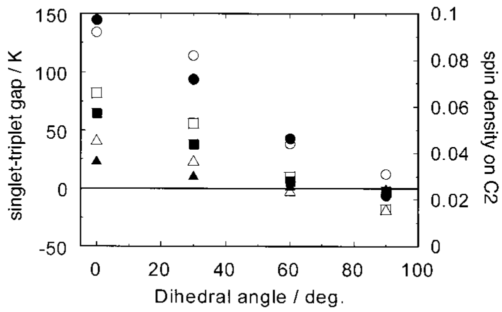


Figure 4. Computed angular dependence (B3LYP method) of the singlet–triplet splitting (filled symbols, left scale) and of the spin density of the $\alpha$-C on the phenyl ring (open symbols, right scale) expressing the twist of a radical fragment with respect to the *m*-phenylene ring for: ○ **diNN-H**; □ **INNN-H**; △ **diIN-H**.

Table 3. B3LYP computated singlet–triplet gaps (S–T) and spin density $\rho_{C2}$ on the carbon C2 for the non-substituted biradicals.

| Dihedral angle | **diNN-H** | | **INNN-H** | | **diIN-H** | |
|---|---|---|---|---|---|---|
| | S–T(K) | $\rho_{C2}$ | S–T(K) | $\rho_{C2}$[a] | S–T(K) | $\rho_{C2}$ |
| 0 | +145 | 0.092 | +65 | 0.076/0.066 | +24 | 0.046 |
| 30 | +90 | 0.082 | +38 | 0.065/0.053 | +1 | 0.037 |
| 60 | +43 | 0.044 | +6 | 0.043/0.030 | +2 | 0.024 |
| 90 | −6 | 0.031 | −2 | 0.028/0.016 | −0.1 | 0.016 |

[a] The two values indicate the spin density on the carbon next to the **NN** radical and the **IN** radical, respectively.

the variation of the strength of the intramolecular interactions can not be attributed solely to the spin polarisation effect, as the S–T gap is known to depend in similar biradicals on the changes in the values of the torsion angle of the radical cycles with respect to the phenyl ring. As the geometry of the isolated biradicals in the solution media is not known experimentally, we have to evaluate the variation of the S–T gap with the torsion angle between the five and six-membered rings for all conformations which are energetically available to the biradical at room temperature. We computed the relative stability of the various conformations by twisting simultaneously and the five-membered rings in the same direction around the C–C bond which links the five- and six-membered rings. The geometry of the molecule was optimised at each point. The most stable conformation in all biradicals is that in which the two five-membered rings are coplanar (see Supporting Information). The stability of the biradical decreases in a continuous way as the torsion angle is increased up to their maximum, located at 90°. The barrier height in the **diNN-H**, **INNN-H** and **diIN-H** is 30, 37 and 22 kcal mol$^{-1}$, respectively. Therefore, only those conformations in the 0–40° angular range are energetically available in solution at room temperature (if the solvent does not present specific interactions with the biradicals). The variation of the S–T gaps and the atomic spin population on the C2 atom with the torsion angle are plotted against the torsion angle in Figure 4 and their values are reported in Table 3. The S–T gap becomes smaller for larger twist angles. A similar decrease with the torsion angle is found for the atomic spin population on the C2 atom, again indicative of a correlation between the values of the S–T gap and the size of the atomic spin population on the *m*-phenylene coupler. When the results of all phenyl coupled radicals computed here are considered, one finds that at the same geometrical conformation the S–T gap increases in the order **IN** < **NN** < ***t*BuNO$^\cdot$** < **HNO$^\cdot$** < **CH$_2$$^\cdot$**, and that this hierarchy corresponds to the parallel increase in the atomic spin population on the C2 atom of the phenyl ring. Therefore, one can conclude that the efficiency of the magnetic coupling, that is, the magnitude of the S–T gap, is related to the amount of atomic spin density on the atom of the C2 atom.

Another important point about the S–T gap is the modification of the ground state when the torsion angle is close to 90°. In these conformations the singlet state becomes the ground state. This has been observed experimentally in various cases of *m*-phenylene with *tert*-butyl nitroxides where the bulky substituents induced such an orthogonal conformation of the radical fragments.[5] The singlet ground state has previously been computed through DFT ab initio calculations for (**1c**, R = $CH_2$) and (**1b**, R = HNO), as reported in Table 2, where the torsion between the radical orbitals and the aromatic ring is 90°.[23] According to these authors, the stabilisation of the singlet state with respect to the triplet state in this peculiar conformation arises from the lifting of the degeneracy of the symmetric and antisymmetrical non-bonding molecular orbital (NBMO) localised at the radical centres. This lift is also found in the **diIN-H**, **INNN-H** and **diNN-H** biradicals.

**Solid-state properties**: In order to rationalise the magnetic properties of molecular compounds, analysis of the molecular packing so as to find out possible magneto–structural correlations is usually carried out. The most common method is to find the shortest intermolecular distance and to consider the signs of the spin densities involved in these contacts according to McConnell's first proposal.[25] However, the results of a statistical analysis have recently pointed out that there is no way of correlating the geometry of one type of contact to the bulk magnetic properties.[9] Furthermore, the reported successful applications of McConnell's first proposal have been shown to result from compensated errors.[26] Nevertheless, the present series of isostructural compounds or compounds with similar molecular packing is expected to allow a careful analysis of the structure-to-magnetic properties. Indeed, the substitution of the **IN** radical by the **NN** radical affects only a few contacts upon suppressing one oxygen atom. Thanks to an appreciable subsequent modification of the magnetic properties, we are able to estimate the relevance of various local molecular arrangements in the set up of magnetic exchange. A way of simplifying the analysis of molecular packing within a crystal structure has been developed in previous studies.[9] It consists in determining the primary, secondary and tertiary patterns related to the strength of the hydrogen bonds in the structure. At intermolecular distances shorter than 5 Å, the contacts are considered between the molecular fragments known to bear the highest spin density, for example, between NCNO or ONCNO groups. These are reviewed within each pattern by consideration of the geometry of the contacts by using the QUEST program of the Cambridge Data Base for crystallographic data. In the present study, such an analysis suggests a pathway for the magnetic exchange and leads to a model for describing the magnetic properties determined with the help of a SQUID magnetometer.

**Series R = H**: The compounds of this series crystallised in the same space group $P2_1/n$ with very similar cell parameters (Table 4). The crystal structure of the **diNN-H** compound has been previously determined.[11] The present analysis confirms the previous data.

In the case of **INNN-H**, disorder is present on the methyl groups of cycle 2 and on the internal oxygen atoms $O_1$ and $O_3$ (Figure 5). For compound **diIN-H**, cycle 2 flips between two extreme positions. These correspond to the limits $-1°$ and $32°$ for the dihedral angle between the phenyl ring and the plane of the ONCNO fragment. In any case, we would like to stress that there is *no* disorder on cycle 1 in the three compounds. The dihedral angle for cycle 1 within **diNN-H** and **INNN-H** is 34°, and 36° in the case of **diIN-H**. Weak hydrogen bonds are represented in the case of the **diNN-H** compound on Figure 5, as previously mentioned by Shiomi et al.[11a] These are: i) along the *a* direction, two contacts between $O_1$ and aromatic hydrogen atoms, as well as two contacts between $O_2$ and the methyl groups of the neighbouring radical (Figure 5a), and ii) along the *c* direction, $O_1$ is linked to a methyl group of the

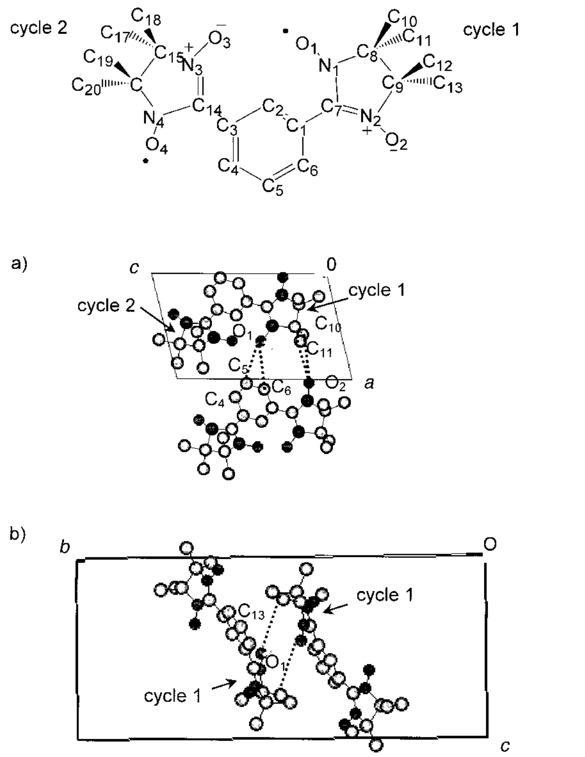


Figure 5. View of the weak hydrogen bonds (···) and of the shortest intermolecular distances involving NO fragments ("magnetic contacts") within: a) **diNN-H** in the *ac* plane; b) **INNN-tmsa** in the *bc* plane.

molecule related by an inversion centre (Figure 5b). It has been shown theoretically that weak hydrogen bonds between an oxygen and an aromatic ring are stronger than those with a methyl group.[9a] From this analysis, the *primary* pattern is made of chains along the *a* axis. The *secondary* pattern builds up a double chain or ribbon owing to the presence of the hydrogen bonds along the *c* axis between two molecules belonging to two neighbouring chains (Figure 6). These ribbons are connected through other weak hydrogen bonds which are affected by disorder on cycle 2.

It is worth recalling that the spin density is mostly distributed over the ONCNO fragments of the imidazolyl rings. Within the primary patterns, only one contact is found with the imidazolyl ring along *a* between $O_1$ and $O_2$, at 4.33 Å for **diNN-H** and 4.29 Å for **INNN-H** (contact 1). Obviously, this contact is not present in the **diIN-H** compound, owing to the absence of $O_2$. Analysing the secondary patterns, a short contact is observed at 3.52–3.56 Å (contact 2) in all cases between $O_1$ of neighbouring molecules. Moreover, these contacts have a similar geometry for the three compounds, and they exclusively involve cycle 1, which does not show

Table 4. Crystallographic data of the biradicals (*r* means the number of unique reflections observed).

| | diIN-H | INNN-H | diNN-tmsa | INNNtmsa | diNN-tr | DiIN-tr |
|---|---|---|---|---|---|---|
| formula | $C_{20}H_{28}N_4O_2$ | $C_{20}H_{28}N_4O_3$ | $C_{25}H_{36}N_4O_4Si \cdot CH_2Cl_2$ | $C_{25}H_{36}N_4O_3Si$ | $C_{22}H_{28}N_4O_4$ | $C_{22}H_{28}N_4O_2$ |
| *M* | 356.47 | 372.47 | 569.12 | 468.68 | 412.49 | 380.49 |
| crystal system | monoclinic | monoclinic | orthorhombic | monoclinic | monoclinic | monoclinic |
| space group | $P2_1/n$ | $P2_1/n$ | *Pbca* | $P2_1/n$ | $P2_1/n$ | $P2_1/n$ |
| *a* [Å] | 7.1575(4) | 7.2287(7) | 15.2687(4) | 11.8660(5) | 12.6111(4) | 12.1503(8) |
| *b* [Å] | 25.553(2) | 25.462(4) | 13.2877(3) | 21.5240(5) | 11.1302(9) | 10.7762(6) |
| *c* [Å] | 11.5030(7) | 11.596(1) | 30.1885(8) | 10.9600(5) | 16.1534(8) | 16.6926(7) |
| $\beta$ [°] | 102.430(5) | 103.793(7) | 90 | 109.717(1) | 97.604(4) | 96.778(4) |
| *V* [Å³] | 2054.6(4) | 2072.8(8) | 6124.8(5) | 2635.1(3) | 2247.4(4) | 2170.4(4) |
| *Z* | 4 | 4 | 8 | 4 | 4 | 4 |
| $\rho$ [g cm$^{-3}$] | 1.15 | 1.19 | 1.24 | 1.18 | 1.22 | 1.16 |
| *r* | 4472 | 4651 | 7394 | 20386 | 4974 | 4804 |
| r, $I > 2\sigma$ | 2028 | 1615 | 4026 | 4191 | 2528 | 2160 |
| *R(I)* | 0.136 | 0.103 | 0.076 | 0.050 | 0.061 | 0.116 |
| $R_w(I)$ | 0.165 | 0.119 | 0.096 | 0.060 | 0.091 | 0.136 |

  0947-6539/01/0711-2472 $ 17.50+.50/0 *Chem. Eur. J.* **2001**, *7*, No. 11

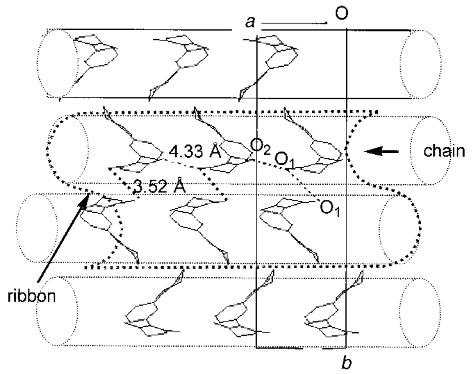


Figure 6. Representation of the different patterns (primary, secondary, tertiary) depicting the molecular packing within the **diNN-H** crystal structure in the *ab* plane (see text).

any disorder. The tertiary patterns do not show any contact shorter than 5 Å. According to the pathways defined by the considered "magnetic contacts", the molecular packing is made up of dimers. These are isolated in the case of **diIN-H**, or related through a longer contact in the case of **diNN-H** and **INNN-H**. The magnetic behaviour of the three compounds is reported in Figure 7. As expected for such biradicals, the $\chi T$

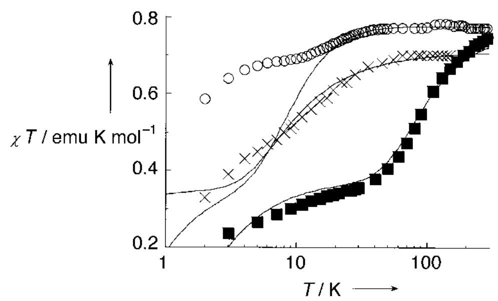


Figure 7. Temperature dependence of the magnetic susceptibility (determined by SQUID magnetometry, $\chi T$ product) of polycrystalline samples for: ○ **diNN-H**; × **INNN-H**; ■ **diIN-H**. Solid lines are the fits of the experimental data (see text).

product is close to 0.75 emu K mol$^{-1}$ at room temperature. The decrease of $\chi T$ with a decrease in temperature reveals a predominant antiferromagnetic intermolecular interaction, since the intramolecular ferromagnetic exchange has been determined in the previous section. Because the intramolecular exchange is different for the three compounds, the different magnetic behaviours could be owing to both different intermolecular and intramolecular couplings. In order to determine the influence of contact **1** within the **INNN-H** and the **diNN-H** crystals, the three molecular packings are considered as made of isolated dimers of biradicals. This is sketched by the four-spins model in Scheme 2 with $J_1$ as the intramolecular coupling constant and $J_2$ as the intermolecular coupling constant.

This model has been previously considered by Shiomi et al. for **diNN-H**,[11a] although it could not reproduce the low temperature behaviour. In this compound, a structural distortion has been further shown below 30 K.[27] A model of isolated dimers with two nonequivalent dimers represents the low temperature region of the susceptibility. However,

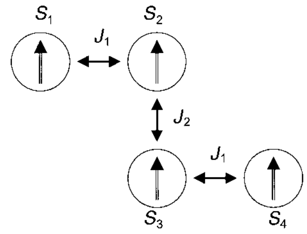


Scheme 2. Four-spins model as a result of isolated dimers of biradicals: $J_1$, intramolecular coupling constant; $J_2$, intermolecular coupling constant.

given this assumption, the magnetic behaviour above 30 K should be owing solely to the equivalent isolated dimers depicted in Scheme 2. Therefore, the four-spins model[28] should be valid within the 30–300 K temperature range. The results of this analysis for the three compounds are: i) $J_1/k_B = 7.2 \pm 0.9$ K, $J_2/k_B = -10.8 \pm 0.7$ K for **diNN-H** within the 30–300 K temperature range, ii) $J_1/k_B = -1.6 \pm 0.6$ K, $J_2/k_B = -8.6 \pm 0.8$ K for **INNN-H**, iii) $J_1/k_B = 25.0 \pm 1.0$ K, $J_2/k_B = -90.0 \pm 2.1$ K for **diIN-H**. For these last two compounds, the fit has been performed within the 2–300 K temperature range, as justified in the crystal studies performed by EPR. Numerically, a study of the goodness of the fits and sensitivity to modifications of the parameters within the same model shows that only the values found for **diIN-H** may be considered as stable. This is expected owing to the large negative $J_2$ suggested for this compound, hence yielding a great sensitivity of the fit to its value. Notably the intramolecular coupling for all compounds disagree with the values found for the isolated molecules. Although the occurrence of disorder allows the variation of $J_1$ between extreme values, the average value should be larger in the case of **diNN-H** according to the theoretical studies and to the value of 23 K found for a similar molecular conformation within a solid.[11c] The value of $J_1$ is obviously wrong in the case of **INNN-H**, since the singlet ground state is suggested for this biradical in disagreement with all of our results. The value of $J_1$ for **diIN-H** appears to be overestimated with respect to both the experimental and theoretical results for the isolated molecule. Moreover, the contact **2** is identical in the three compounds. This is in contrast to the large difference found for the $J_2$ values of the three compounds. The strong negative value of $J_2$ found for the **diIN-H** compound is in agreement with the head-to-tail disposition that provides a good overlapping of the SOMOs generally assumed to result in an antiferromagnetic exchange.[29] From the structural analysis it can be shown that only the **diIN-H** compound may be represented by an isolated four-spins model. This is in qualitative agreement with the present results. The couple of ($J_1$, $J_2$) values found for **diIN-H** is consistent with the magnetic behaviour and with the structural analysis. However, owing to the disorder, this must be considered as a rough average. According to the structural analysis which shows the existence of contact **1** within **diNN-H** and **INNN-H**, the failure of the isolated four-spins model to represent their magnetic behaviour is well understood. Although the present analysis for the **diNN-H** compound does not disagree with the previous studies, it suggests that the intermolecular interactions owing to the contact **1** should be considered within the

  0947-6539/01/0711-2473 $ 17.50+.50/0 

whole 30–300 K temperature range. Chains of dimers of biradicals are suggested for the magnetic behaviour of **diNN-H** and **INNN-H**, that is, chains with quintet spin states, the numerical results are not available.

The anisotropy of the EPR response has been investigated on oriented single crystals in order to reveal possible low dimensional (low-D) magnetic behaviour.[3e, 30] The principal values of the $g$ tensor are in agreement with the previous determination for **diNN-H.**[11b] They are determined for i) **diIN-H**: $g_1 = 2.0073_4$, $g_2 = 2.0075_7$, $g_3 = g_b = 2.0041_9$ ($g_{av} = 2.0063_7$), and ii) **INNN-H**: $g_1 = g_b = 2.0043_0$, $g_2 = 2.0082_4$, $g_3 = 2.0075_8$ ($g_{av} = 2.0067_1$). In agreement with the comparable molecular packing, a similar angular dependence with comparable values for the absorption linewidth ($\Delta B_{1/2}$) is observed for the three compounds. This could not be correlated to a peculiar low-D magnetic behaviour. However, the temperature dependence of the shape of the EPR spectra reveals that it remains symmetrical, close to the Lorentzian shape throughout the whole temperature range (4–300 K) for **INNN-H** and **diIN-H**, whereas strong deviation from this shape is observed for **diNN-H** below 30 K.[31] This observation must be related to the structural distortion previously found in this compound.[27] Hence, the lack of distortion of the EPR line-shape within the same temperature range for the two other compounds may be considered to exclude such a phenomenon, as in the previous discussion of the static susceptibility. A peculiar behaviour is revealed by the study of the temperature dependence of $\Delta B_{1/2}$ along the crystallographic axes. Changes in the temperature dependence of the linewidth are observed at temperatures where a change is observed in the susceptibility, for example, the limits of a plateau or beginning of a decrease in the $\chi T$ product (Figure 8).

It is worth recalling that the behaviour of the EPR linewidth is mainly governed by the dipolar interactions, that is, the disposition of the NO groups in the present biradical derivatives. As pointed out in the analysis of the crystal packing, the NO groups of cycle 2 show a strong disorder at high temperature. It is suggested that the present results indicate the molecular ordering of the imidazolyl cycles as the temperature decreases. According to this proposal, a preferential position is progressively adopted by the NO groups. In the case of **diNN-H**, this is observed below approximately 30 K and it has been related to the structural distortion previously observed as discussed already. A minimum of $\Delta B_{1/2}$ occurs by approximately 10–20 K for **INNN-H**, and by approximately 40–50 K for **diIN-H**. For **diIN-H**, a second change is observed by approximately 20 K. The present proposal may explain the failures to simulate accurately the magnetic behaviour of the three compounds, even in the expected simplest case of the **diIN-H** compound.

**Series R = tmsa**: Only the crystal structures of **diNN-tmsa** and **INNN-tmsa** have been determined (Table 4). The **diNN-tmsa** crystal accommodates the solvent dichloromethane in a 1:1 ratio and the asymmetric unit does not exhibit any disorder. The dihedral angles between the phenyl and the imidazolyl rings are 24° and 30°. Following the previously described procedure for the analysis of the crystal packing, the primary

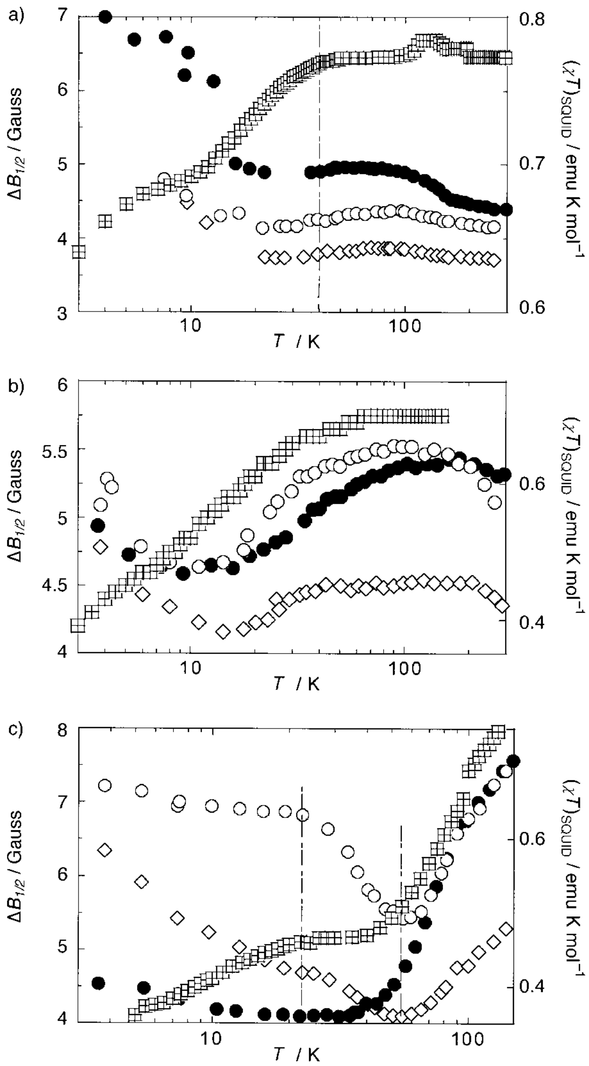


Figure 8. Temperature dependence of EPR absorption linewidth (left scale) along the crystalline axes of single crystals (●, $a$ axis; ○, $b$ axis; ◇, $c^*$ axis) compared with the magnetic susceptibility (determined by SQUID magnetometry on polycrystalline samples, ⊞ $\chi T$ product on the right scale) for: a) **diNN-H**; b) **INNN-H**; c) **diIN-H**.

patterns consists of dimers within the $ab$ plane. These dimers make chains along the $ab$ direction, to give the secondary patterns (Figure 9a). The connection of these chains yields planes parallel to the $ab$ plane, thus defining the tertiary structure.

Within the dimers, two symmetrical groups of short contacts are associated in the proximity of the NO group $N_1O_1$ of one molecule to the ONCNO fragment of the head-to-tail neighbouring molecule. Among them, we observe i) a contact $O_1 \cdots O_3$ at 3.73 Å, ii) a contact $O_1 \cdots O_4$ at 4.06 Å, iii) a contact $O_1 \cdots C_{14}$ at 3.03 Å (Figure 9a). Within the chains, two $O_1 \cdots O_4$ contacts of different geometry are present at 3.98 Å and 3.87 Å between molecules of two different dimers. Between the chains and between the {110} family of planes, the intermolecular distances are larger than 6 Å. These contacts have been neglected. Within the **INNN-tmsa** compound, the imidazolyl cycles are nearly planar with respect to the benzene ring, with dihedral angles of 0° and 1°. A disorder is observed for the oxygen atoms, as previously described for

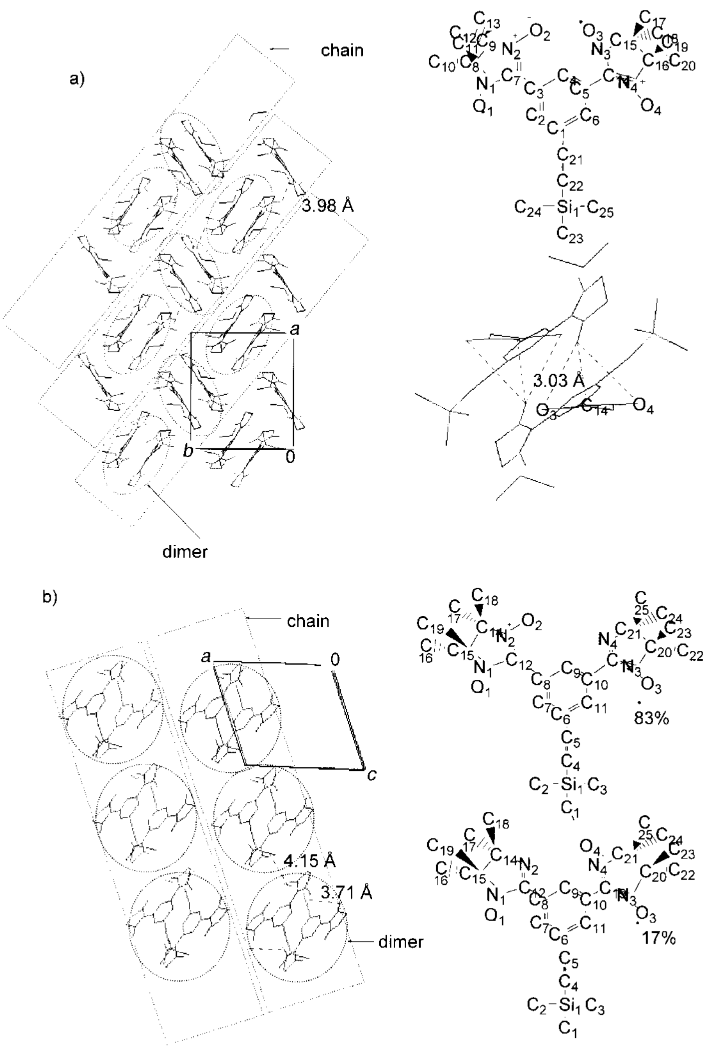

Figure 9. Representation of the different patterns (primary, secondary, tertiary) depicting the molecular packing within a) the **diNN-tmsa** crystal structure in the *ab* plane. b) the **INNN-tmsa** crystal structure in the *ac* plane.

the **INNN-H** compound. From the isotropic thermal factors, the probability for the **IN** fragment to be in the position of cycle 1 is estimated at 17% (deduced from the isotropic thermal factors), and 83% in the position of cycle 2 (Figure 9b). According to these data, in all cases, the oxygen atom of **IN** is localised in $O_1$ or $O_3$ position. Considering the weak hydrogen bonds, the structure is considered as an assembly of head-to-tail dimers (primary patterns), associated into chains along the *c* direction (secondary patterns) which connect into planes parallel to the *ac* plane (tertiary patterns) (Figure 9).

Within the dimers, short contacts are measured between the sites of high spin density: i) $O_3 \cdots O_1$ contact at 3.71 Å, ii) $N_3 \cdots O_1$ contact at 3.51 Å, and iii) $O_3 \cdots N_1$ contact at 3.77 Å. Only one short contact is present within the chains and between dimers at 4.15 Å ($O_2 \cdots O_2$).

The magnetic properties of the three synthesised derivatives are reported in Figure 10. For **diNN-tmsa**, a maximum of the $\chi T$ product is observed at 8 K with the value of 1.2 emu K mol$^{-1}$ (Figure 10a). For the **diIN-tmsa** and **INNN-tmsa** compounds, a continuous decrease of $\chi T$ is observed as the temperature decreases (inset in Figure 10b). A maximum is observed in the susceptibility close to 50 K for both compounds.

In the case of the **diNN-tmsa** compound, the maximum of $\chi T$ is larger than the expected maximum value for isolated biradicals (1 emu K mol$^{-1}$). Hence, a *ferromagnetic intermolecular* interaction must be involved within the primary

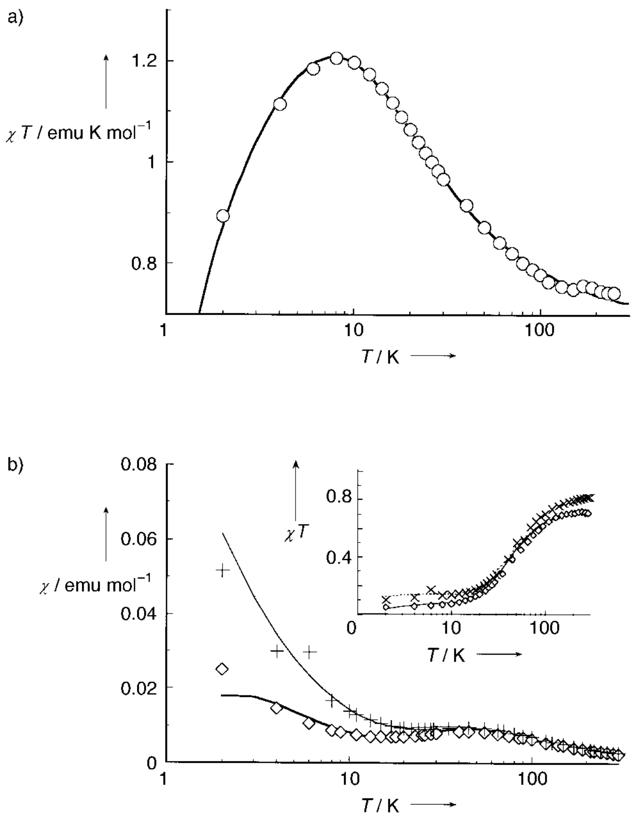

Figure 10. Temperature dependence of the magnetic susceptibility (determined by SQUID magnetometry, $\chi T$ product) of polycrystalline samples for: a) **diNN-tmsa**; b) ◇ **INNN-tmsa**, + **diIN-tmsa**. Solid lines are the fits of the data (see text).

patterns. A short contact between the central carbon atom of ONCNO and a NO group have been previously considered to set up ferromagnetic intermolecular interactions.[32] It would be more convenient to say that the relative disposition of the imidazolyl cycles gives an assembly of contacts, of which this contact is the shortest. This relative disposition can be proposed as giving rise to this ferromagnetic interaction. In the case of **INNN-tmsa**, the analysis of the structure reveals only short NO···NO contacts. The geometry is particularly favourable to the overlapping of SOMOs, since the NO groups are parallel to each other, and in the case of the interdimer contact, are strictly coplanar. The shortest contacts are always present within the dimers, since they involve oxygen atoms without disorder, whereas the interdimer contact involves $O_2$ atoms that are statistically present. The modelling of these behaviours could be carried out in the same way for both **INNN-tmsa** and **diNN-tmsa**, since the packings may be considered from a magnetic point of view as assemblies of dimers weakly connected. The contacts within

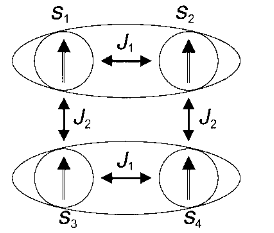


Scheme 3. Symmetrical four-spin system as a result of contacts within the dimers involved the four imidazolyl cycles.

the dimers involved the four imidazolyl cycles, leading to a symmetrical four-spin system represented in Scheme 3.[28]

The magnetic behaviour of **diNN-tmsa** is well represented by this model, taking into account the interdimers interactions by a mean-field approximation. The values obtained are: $J_1/k_B = 17.4 \pm 1.0$ K; $J_2/k_B = 11.4 \pm 0.5$ K; $\theta = -0.7 \pm 0.1$ K. The intramolecular magnetic coupling is in good agreement with the estimation for the isolated molecule. Moreover, the intermolecular ferromagnetic interaction of $J_2/k_B = 11.4$ K is of the same magnitude of the previously reported values for compounds which exhibit a similar type of contact.[32] However, this model fails to represent the behaviour of **INNN-tmsa**, particularly in the low temperature region. In order to impose a physical solution among various couples of parameters that result from the fitting procedure, the intramolecular coupling constant $J_1$ has been fixed. It is important to notice that i) the value of $J_1$ has little influence on the high temperature behaviour of the fit, and ii) the position of the maximum of the susceptibility mainly depends on the value of $J_2$. For **INNN-tmsa** compound, $J_1/k_B = 20$ K has been fixed according to the experimental determination. This fitting procedure has been followed within the 50–300 K temperature range. It gives an estimation of the intermolecular antiferromagnetic interaction range as $J_2/k_B = -37.5 \pm 0.3$ K. Although the above simulation represents accurately the data within the 50–300 K range, particularly the position of the maximum, the lower temperature region is not described at all. The observed behaviour cannot be attributed to monoradical impurities since in this case those impurities would be in the order of 15–20% to reproduce the data. There are no facts favouring such an assumption. Moreover, since both **INNN-tmsa** and **diIN-tmsa** exhibit the same anomaly, the assumption of a damaged sample is rather poor. Finally, one may wonder why such phenomena are not observed in the previous derivatives. In order to explain such low temperature behaviour, the presence of some *isolated* biradicals has to be considered. This can be obtained by removal of both contacts within the dimer, hence assuming the lack of the oxygen atoms in position $O_1$ or $O_3$, owing to the disorder. Consideration of the probabilities obtained from isotropic thermal factors gives only a rough idea of the probability of presence, we have performed various simulations with slight modifications of the probability such as, for example 94% on $O_1$, 94% on $O_3$, 89% on $O_2$ and 23% on $O_4$ instead of the 100%, 100%, 83% and 17% found from the isotropic thermal parameters. This situation leads to a mixture of three different models, that is, 78.1% of a symmetric four-spins model, 21.2% of a four-spins linear model (only one $J_2$ interaction), and 0.7% of isolated biradicals (only $J_1$).[33] We used the same parameters as in the above part, that is, $J_1/k_B = 20$ K and $J_2/k_B = -40$ K, to see the influence of the disorder on the susceptibility. Indeed, this simulation reproduces quite well the features of the magnetic behaviour of **INNN-tmsa** as shown in Figure 10b. In the case of **diIN-tmsa**, the great similarity of magnetic behaviour strongly supports a similar type of packing. Assuming a disorder on the oxygen atoms as, for axample, 90% on $O_1$, 90% on $O_3$, 10% on $O_2$ and 10% on $O_4$, the situation is then described as 65.61% of a symmetric four-spins model, 30.78% of a four-spins linear model, and 3.61% of isolated biradicals.[32] The simulation with $J_1/k_B = 10$ K (as expected for a **diIN-R** biradical) and $J_2/k_B = -40$ K reproduces well the magnetic data of **diIN-tmsa**, as seen in Figure 10b. The magnetic behaviour of these two compounds has thus been shown to be governed by a strong antiferromagnetic intermolecular interaction close to $-40$ K, due to the NO···NO short contacts, and the peculiar features of the magnetic susceptibility can be well described taking into account the disorder on the oxygen atoms.

**Series R = triple bond**: The crystal structures of **diNN-tr** and **diIN-tr** were determined (Table 4). The asymmetric unit for both compounds does not exhibit disorder, except for the methyl groups within **diIN-tr**. The dihedral angles between the phenyl and the imidazole rings are 25° and 42° for **diNN-tr**, 28° and 36° for **diIN-tr**. Considering the weak hydrogen bonds, the primary pattern consists of chains along the *b* axis. The molecules are linked through a hydrogen bond between the acetylenic unit and the oxygen atom $O_1$ in the case of **diNN-tr**. This contact involves the nitrogen atom $N_1$ for **diIN-tr**. The C(sp)—H···X (X = N or O) angle is 169° and 146° for **diNN-tr** and **diIN-tr**, respectively. This is in agreement with the angle values found for these types of weak hydrogen bonds.[7] The secondary patterns are formed by the connection of these chains along the *a* axis, giving rise to parallel planes with respect to the *ab* plane (Figure 11a). The tertiary structure is obtained by connecting these planes along the *c* axis by two types of $C(sp_3)-H \cdots O$ contacts.

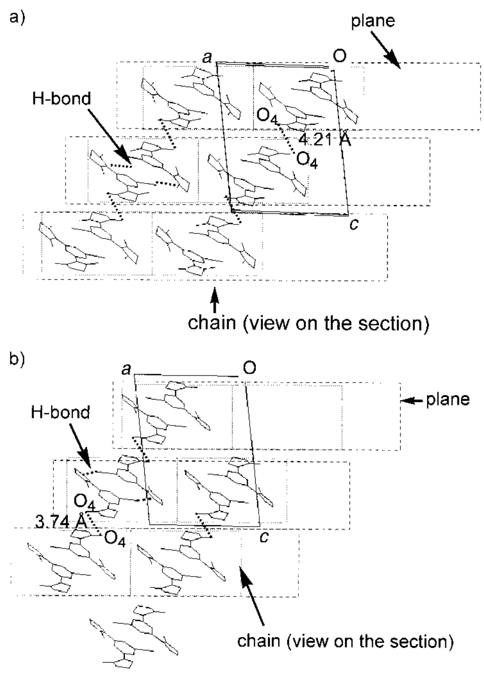


Figure 11. Representation of the different patterns (primary, secondary, tertiary) depicting the molecular packing within the *ac* plane of the crystal structure of: a) **diNN-tr**; b) **diIN-tr**.

Following our methodology, the geometry of the short contacts in the ONCNO regions has been investigated. In the **diNN-tr** chains, the short contacts are: $N_1 \cdots O_3$ at 3.70 Å, $O_1 \cdots O_3$ at 3.98 Å, and $N_2 \cdots O_3$ at 4.12 Å. The only short contact within the chain for **diIN-tr** occurs between $N_3$ and $O_1$ at 4.40 Å. Between the chains, within the *ab* planes, no short contact could be found at shorter distances than 5 Å in either of the two compounds. Between the planes, the $N_4 \cdots O_4$ contact build up dimers, with a short distance of 3.74 Å for **diIN-tr** and 4.09 Å for **diNN-tr** (Figure 11bb). The NO groups are related by an inversion centre, which gives rise to the coplanarity of the two NO groups and a good overlapping of the SOMOs as already discussed in the derivatives bearing R = tmsa. Therefore, the structure may be considered as chains along the *b* axis with a loose interchain connection along *c* for **diNN-tr**. In the case of **diIN-tr**, the situation is that of nearly isolated dimers. This is supported by the difference in the spin density distribution between an **IN** and a **NN** radical, as demonstrated by neutron diffraction experiments.[34] The smaller spin density on the nitrogen atom $N_1$ and the larger spin density on the $N_4 \cdots O_4$ for the **IN** radicals as compared with the **NN** radicals induces a weaker through-chain interaction and a stronger interaction within the dimers for **diIN-tr** as compared with **diNN-tr**. At room temperature, the value of $\chi T$ is 0.75 emu K mol$^{-1}$ for both compounds, in agreement with two independent $S = ½$ spins (Figure 12).

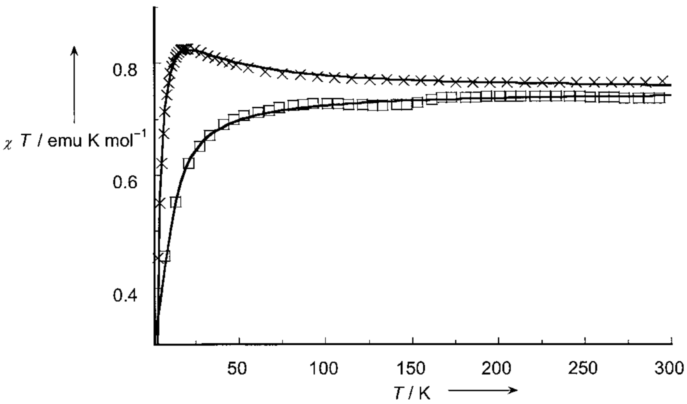


Figure 12. Temperature dependence of the magnetic susceptibility (determined by SQUID magnetometry, $\chi T$ product) of polycrystalline samples for: a) ×, **diNN-tr**; b) □, **diIN-tr**. Solid lines are the fits of the experimental data (see text).

For the **diIN-tr** compound, antiferromagnetic interactions dominate the behaviour at low temperature as inferred from the decrease of $\chi T$. For **diNN-tr**, a maximum is observed by approximately 20 K with a value of 0.84 emu K mol$^{-1}$. Such a ferromagnetic interaction is attributed to the intramolecular magnetic exchange as expected from the results on the isolated biradicals. The decrease of $\chi T$ at lower temperature indicates the competition between intermolecular antiferromagnetic interactions and the intramolecular ferromagnetic interaction. The magnetic behaviour of **diIN-tr** may be simulated as isolated dimers of biradicals, that is, the linear four-spins system (Scheme 3), although the smooth variation does not allow an accurate determination of the intramolecular $J_1$. As expected from our results, this turns out to be small within a **diIN-R** derivative. The fitting procedure is rather insensitive to a small variation of the couple of parameters. The values of $J_1$ may be chosen within the $-5$–$+5$ K range, and the values of $J_2$ may be chosen within the $-15$–$-5$ K range. Therefore, the antiferromagnetic interaction as a result of the head-to-tail stacking is much weaker than the similar one found in the case of **diIN-H** ($J_2/k_B \approx -90$ K). A comparison of the geometry of the dimer within the two derivatives shows that both have exactly the same geometrical parameters, except for the nearest neighbour distance within the dimer. The nearest neighbour distance is larger by 0.2 Å within **diIN-tr**. Hence, the comparison of the two compounds gives a nice illustration of the effect of the distance on the magnetic exchange: The value of $J_2$ is about nine times larger on decreasing the distance from 3.74 down to 3.54 Å. For **diNN-tr**, a nearly isolated alternating chain model does correspond to the structural analysis, with $J_1$ as the ferromagnetic intramolecular interaction, and the antiferromagnetic intermolecular interactions are associated to $J_2$ (Scheme 4).[35]

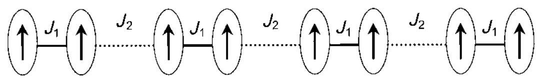


Scheme 4. Structural analysis for **diNN-tr**: $J_1$, ferromagnetic intramolecular interaction; $J_2$, antiferromagnetic intermolecular interactions.

The proposed model gives a satisfactory representation of the experimental data with the parameters $\alpha = J_2/J_1 = 5.8 \pm 0.2$, and $J_2/k_B = -4.0 \pm 0.1$ K, thus yielding $J_1/k_B = 23.2 \pm 1.4$ K. The estimation of the intramolecular $J_1$ is in good agreement with the results of the studies of isolated molecules. The dihedral angles of 25° and 42° are indeed quite close to the one of 30° measured for **diNN-H** in previous studies affording an estimation of $J_1$ of 23 K.[11c]

## Conclusion

The intramolecular exchange coupling between **IN** and or **NN** radical substituents within biradical derivatives based on the *m*-phenylene moiety has been properly assessed (strength and sign) in the isolated state with the help of the EPR technique. These results are further reinforced and extended by the results of ab initio calculations. The main conclusions are: i) The triplet is the magnetic ground state for all derivatives except when the molecular conformation involves the orthogonal radical fragments, and ii) the singlet–triplet splitting depends on the radical substituent: It increases on substitution of **IN** by **NN**. This effect is attributed to the difference in the spin polarisation mechanism between these biradicals. This tends to increase the spin density distribution over the coupling unit, hence increasing the through-bond magnetic exchange. The aim to obtain single crystals of isostructural compounds made of chemically similar molecules has been successful. A careful and precise study of the crystal structures has been conducted following a previously developed strategy and the intermolecular contacts have been rationalised.[9] The results of such analyses enable us to simulate successfully the magnetic behaviour of most compounds. In particular, the magnetic properties of the biradicals are either confirmed, or used as a check of the validity of the proposals. When the model was not satisfactory, we have considered the failures objectively. As a summary, soft changes in the crystal packing, for example, addition/removal of only a few relevant contacts, enables the rationalisation of the pathways for the set up of magnetic exchange. According to recent theoretical studies and statistical analyses,[9] the relation between structure and magnetism requires consideration of the relative disposition of all the molecules in the crystal. This paper shows that the comparison of peculiar patterns is an objective way to deduce magnetic pathways. It is believed that the studies of basic bricks, such shown here (biradicals and the corresponding dimers and/or tetramers), are of utmost importance to understand more complex systems. An extension of this work including triradicals and tetraradicals based on these bricks will be described elsewhere.

## Experimental Section

**Materials and methods**: Solvents were distilled before use. In particular, THF was dried over sodium/benzophenone, diisopropylamine over KOH and distilled under Argon. All the reagents were used as received. Trimethylsilylacetylene was purchased from LANCASTER, isophthalic acid from ALDRICH. Thin-layer chromatography (TLC) was performed on aluminium plates coated with Merck silica gel 60 $F_{254}$. Microanalyses were performed by the Service d'Analyse de l'Institut Charles Sadron. Fast-atom bombardment (FAB, positive mode) were recorded on a ZAG-HF-VG-Analytical apparatus in a *m*-nitrobenzyl alcohol (*m*-NBA) matrix. $^1$H and $^{13}$C NMR spectra were recorded on a Bruker ARX 300 spectrometer. The EPR spectra have been recorded on an X-band Bruker spectrometer (ESR-300) equipped with a rectangular TE 102 cavity. The static magnetic field was measured with an NMR gaussmeter (Bruker ER035) while the microwave frequency was measured with a frequency-meter (HP-5350 B). The studies of the angular dependence of the EPR response of the single crystals were carried out with the aid of a one-axis goniometer (Bruker ER218G1). Solutions were degassed by bubbling argon directly in the EPR tube prior to measurements. Temperature was measured by a thermocouple introduced inside the tube, at 1.5 cm from the bottom. Polystyrene matrices were obtained by lyophilisation of the benzene solutions containing the samples. Magnetic susceptibility measurements were obtained with a Quantum Design SQUID magnetometer.

Crystallographic data (excluding structure factors) for the structures reported in this paper have been deposited with the Cambridge Crystallographic Data Centre as supplementary publication no. CCDC-151350–151354, 151569. Copies of the data can be obtained free of charge on application to CCDC, 12 Union Road, Cambridge CB21EZ, UK (fax: (+44)1223-336-033; e-mail: deposit@ccdc.cam.ac.uk).

**1,3-Bis(1,3-dihydroxy-4,4,5,5-tetramethylimidazolin-2-yl)benzene (4)**: 2,3-Bis(hydroxylamino)-2,3-dimethylbutane (1530 mg, 10.33 mmol) was added to a solution of isophthalaldehyde (604 mg, 4.50 mmol) in MeOH (10 mL). The mixture was stirred for 1 d at room temperature and then concentrated by a slow bubbling of argon to almost dryness over 3 d. The white precipitate was washed with MeOH, leading to a white solid (90%). $^1$H NMR ([D$_6$]DMSO): $\delta = 7.80$ (s, 4H, OH), 7.78–7.47 (m, 4H, Ph), 4.50 (s, 2H, -H imid.), 1.07 (s, 12H, $CH_3$), 1.03 (s, 12H, $CH_3$); $^{13}$C NMR ([D$_6$]DMSO): $\delta = 148.3$, 141.1, 127.2, 115.1 (Ph), 91.0 (CH imid.), 66.0 ($C_{quat}$ imid.), 24.1 ($CH_3$), 17.0 ($CH_3$); elemental analysis calcd (%) for $C_{20}H_{31}N_4O_4$ (391.5): C 60.89, H 8.69, N 14.20; found: C 60.45, H 8.78, N 14.56; IR (KBr): $\tilde{\nu} = 3189$ cm$^{-1}$ (OH).

**1,3-Bis(1-oxyl-3-oxo-4,4,5,5-tetramethylimidazolin-2-yl)benzene (diNN-H)**: $H_2O$ (50 ml) and $NaIO_4$ (337 mg, 1.57 mmol) were added to a suspension of compound **4** (300 mg, 0.76 mmol) in $CH_2Cl_2$ (50 ml). The mixture was stirred at room temperature for 1 h. The organic phase was extracted and dried with $Na_2SO_4$, and the residue was purified by chromatography (silica gel, ethyl acetate/$CH_2Cl_2$ 15:85) to afford the title compound which was recrystallised giving dark blue crystals (253 mg, 86%). M.p. 214 °C (214–215 °C[11b]); IR (KBr): $\tilde{\nu} = 1355$ cm$^{-1}$ (N–O); UV/Vis: $\lambda_{max}$ ($\varepsilon$): 585 nm (835 M$^{-1}$cm$^{-1}$); elemental analysis (%) calcd for $C_{20}H_{28}N_4O_4$ (388.5): C 61.84, H 7.26, N 14.42; found: C 61.80, H 7.29, N 14.41; $N_S = 2.2$ spins per molecule.

**1,3-Bis(1-oxyl-4,4,5,5-tetramethylimidazolin-2-yl)benzene (diIN-H)**: An aqueous solution (15 mL) of $NaNO_2$ (178 mg, 2.6 mmol) acidified to pH 6 with HCl was added to a solution of **diNN-H** (97 mg, 0.25 mmol) in $CH_2Cl_2$ (15 mL). $NaIO_4$ (55 mg, 0.26 mmol) was added after 5 min and the red solution was extracted after 10 min. After the usual workup, the residue was purified by chromatography (silica gel, ethyl acetate/$CH_2Cl_2$ 2:98) to afford a red solid which was recrystallised to red needles (66 mg, 74%) by slow evaporation of a $CH_2Cl_2$/hexane mixture. M.p. 145 °C (142–143 °C[15]); IR: $\tilde{\nu} = 1376$ (N–O), 1549 cm$^{-1}$ (C=N); UV/Vis $\lambda_{max}$ ($\varepsilon$): 444 nm (950 M$^{-1}$cm$^{-1}$); elemental analysis (%) calcd for $C_{20}H_{28}N_4O_2$ (356.5): C 67.39, H 7.91, N 15.71; found: C 67.41, H 7.95, N 15.75; $N_S = 2.0$ spins per molecule.

**1-(1-Oxyl-4,4,5,5-tetramethylimidazolin-2-yl)-3-(1-oxyl-3-oxo-4,4,5,5-tetramethylimidazolin-2-yl)benzene (INNN-H)**: $NaNO_2$ (71 mg, 0.12 mmol) was added to $CH_2Cl_2/H_2O$ 1:1 (100 mL), acidified to pH 6 by HCl, and containing **diNN-H** (200 mg, 0.51 mmol). The reaction was followed by TLC (silica gel, ethyl acetate/$CH_2Cl_2$ 5:95). The colour of the mixture turned from blue to light brown. After 20 min, **diIN-H** and **INNN-H** were predominant in the mixture. The organic phase was quickly isolated, dried on $Na_2SO_4$ and evaporated. After chromatography (silica gel, ethyl acetate/$CH_2Cl_2$ 5:95), a dark grey solid was isolated. Recrystallisation by slow evaporation in a $CH_2Cl_2$/hexane mixture led to black needles (45 mg, 23%). M.p. 183 °C; IR (KBr): $\tilde{\nu} = 1371$ (N–O), 1552 cm$^{-1}$ (C=N); UV/Vis: $\lambda_{max}$ ($\varepsilon$) = 444 (660), 585 nm (510 M$^{-1}$cm$^{-1}$); elemental analysis (%) calcd for $C_{20}H_{28}N_4O_3$ (372.5): C 64.49, H 7.58, N 15.04; found: C 64.38, H 7.63, N 15.08; $N_S = 2.1$ spins per molecule.

**1,3-Bisformyl-5-trimethylsilylacetylenebenzene (2)**: In a 250 mL round-bottomed flask were introduced 1,3-bisformyl-5-bromobenzene[12] (4.0 g, 18.7 mmol), [$PdCl_2(PPh_3)_2$] (395 mg, 0.56 mmol, 3%) and CuI (107 mg, 1%). Under argon, freshly distilled THF (100 mL) and diisopropylamine (20 mL) were added. After addition of trimethylsilylacetylene (3.8 mL, 27.4 mmol, 1.5 equiv), the mixture was stirred at room temperature for 12 h. The ammonium salt was removed by filtration and the filtrate was evaporated to give a crude product, which was purified by chromatography (silica gel, EtOH/$CH_2Cl_2$ 3:97) to yield a white solid (4.05 g, 94%). $^1$H NMR ($CDCl_3$): $\delta = 10.08$ (s, 2H, CHO), 8.31 (t, 1H, $^3J$(H,H) = 1.5 Hz, Ph), 8.20 (d, 2H, $^3J$(H,H) = 1.5 Hz, Ph), 0.28 (s, 9H, $Si(CH_3)_3$); $^{13}$C NMR ([D$_6$]acetone): $\delta = 191.0$ (CHO), 138.1, 137.1, 129.2, 126.2 (Ph), 103.1 (-C≡C-), 97.1 (-C≡C-), −0.5 ($Si(CH_3)_3$); IR (KBr): $\tilde{\nu} = 2164$ (C≡C), 1706 cm$^{-1}$ (CHO); elemental analysis (%) calcd for $C_{13}H_{14}O_2Si$ (230.3): C 67.79, H 6.13, O 13.89; found: C 67.85, H 6.20, O 13.60.

**1,3-Bis(1,3-hydroxy-4,4,5,5-tetramethylimidazolin-2-yl)-5-trimethylsilylacetylenebenzene (5)**: The same procedure as described for compound **4**, starting from **2** (400 mg 1.7 mmol), 2,3-bis(hydroxylamino)-2,3-dimethylbutane (540 mg, 3.65 mmol) in MeOH (15 mL) was used, and led to a white powder (718 mg, 86%). $^1$H NMR ([D$_6$]acetone): $\delta = 7.66$ (t, 1H, $^3J$(H,H) = 1.5 Hz, Ph), 7.53 (d, 2H, $^3J$(H,H) = 1.5 Hz, Ph), 7.12 (m, 4H, OH), 4.70 (s, 2H, CH imid.), 1.18 (s, 12H, $CH_3$), 1.08 (s, 12H, $CH_3$), 0.25 (s, 9H, Si-$CH_3$); $^{13}$C NMR ([D$_6$]DMSO): $\delta = 142.5$, 126.1, 122.1, 120.1 (Ph), 103.0 (-C≡C-), 92.6 (-C≡C-), 90.0 (CH imid.), 66.1 ($C_{quat}$ imid.), 24.1 ($CH_3$), 17.0 ($CH_3$), −0.2 ($Si(CH_3)_3$); IR (KBr): $\tilde{\nu} = 2155$ (C≡C), 3251 cm$^{-1}$ (OH); elemental analysis (%) calcd for $C_{25}H_{40}N_4O_4Si$ (488.6): C 61.19, H 8.63, N 11.42; found: C 61.35, H 8.75, N 11.78.

**1,3-Bis(1-oxyl-3-oxo-4,4,5,5-tetramethylimidazolin-2-yl)-5-trimethylsilylacetylenebenzene (diNN-tmsa)**: The same procedure as described for compound **diNN-H**, starting from **5** (240 mg, 0.48 mmol) and $NaIO_4$ (230 mg, 1.07 mmol) in $CH_2Cl_2/H_2O$ 1:1 (80 mL) was used. After purification by chromatography (silica gel, ethyl acetate/$CH_2Cl_2$ 10:90), the product was recrystallized in $CH_2Cl_2$/hexane to afford dark blue crystals (174 mg, 75%). M.p. 213 °C; IR (KBr): $\tilde{\nu} = 2158$, (C≡C), 1363 cm$^{-1}$ (N–O); UV/Vis: $\lambda_{max}$ ($\varepsilon$) = 259 (35280), 369 (20635), 589 (790), 617 nm (750 M$^{-1}$cm$^{-1}$); elemental analysis (%) calcd for $C_{25}H_{36}N_4O_4Si$ (484.6): C 61.95, H 7.48, N 11.56; found: C 61.86, H 7.44, N 11.51; FAB$^+$ (*m*-NBA): 484.0 $[M]^+$, 468.1 $[M-O]^+$, 452.1 $[M-2O]^+$, 436.1 $[M-3O]^+$, 420.1 $[M-4O]^+$; $N_S = 2.0$ spins per molecule.

**1,3-Bis(1-oxyl-4,4,5,5-tetramethylimidazolin-2-yl)-5-trimethylsilylacetylenebenzene (diIN-tmsa)**: The same procedure as described for **diIN-H** with **diNN-tmsa** (100 mg, 0.21 mmol) and $NaNO_2$ (145 mg, 2.1 mmol) in $CH_2Cl_2$/$H_2O$ 1:1 (40 mL) was used. After purification by chromatography (silica gel, ethyl acetate/$CH_2Cl_2$ 10:90), the product was recrystallised in $CH_2Cl_2$/hexane to afford red crystals (65 mg, 69%). M.p. 210 °C; IR (KBr): $\tilde{\nu} = 2161$ (C≡C), 1371 (N–O), 1546 $cm^{-1}$ (C=N); UV/Vis: $\lambda_{max}$ ($\varepsilon$) = 301 (5720), 448 nm (822 $M^{-1}cm^{-1}$); elemental analysis (%) calcd for $C_{25}H_{36}N_4O_2Si$ (452.6): C 66.33, H 8.01, N 12.37; found: C 66.05, H 8.07, N 12.20; FAB+ (*m*-NBA): 454.1 $[M+H]^+$, 438.1 $[M-O]^+$, 421.1 $[M-2O]^+$; $N_S = 2.1$ spins per molecule.

**1-(1-Oxyl-4,4,5,5-tetramethylimidazolin-2-yl)-3-(1-oxyl-3-oxo-4,4,5,5-tetramethylimidazolin-2-yl)-5-trimethylsilylacetylenebenzene (INNN-tmsa)**: The same procedure as described for compound **INNN-H** using **diNN-tmsa** (228 mg, 0.47 mmol), $NaNO_2$ (65 mg, 0.94 mmol) in $CH_2Cl_2$/$H_2O$ 1:1 (100 mL) was used. After purification by chromatography (silica gel, ethyl acetate/$CH_2Cl_2$ 5:95), the product was recrystallised in $CH_2Cl_2$/hexane to afford black platelets (46 mg, 21%). M.p. 201 °C; IR (KBr): $\tilde{\nu} = 2161$ (C≡C), 1365 (N–O), 1549 $cm^{-1}$ (C=N); UV/Vis: $\lambda_{max}$ ($\varepsilon$) = 366 (9213), 445 (416), 582 (347), 617 nm (315 $M^{-1}cm^{-1}$); elemental analysis (%) calcd for $C_{25}H_{36}N_4O_3$ (468.6): C 64.07, H 7.74, N 11.95; found: C 64.30, H 7.75, N 12.16; FAB+ (*m*-NBA): 470.1 $[M+H]^+$, 454.1 $[M-O]^+$, 438.1 $[M-2O]^+$, 422.1 $[M-3O]^+$; $N_S = 2.1$ spins per molecule.

**1,3-Bisformyl-5-ethynylbenzene (6)**: $K_2CO_3$ (820 mg, 0.6 mmol) was added under Ar to a solution of **2** (1.40 g, 6.1 mmol) in MeOH (10 mL). The mixture was stirred over 3 h at room temperature. After evaporation of the solvent (*without* heating the bath), $CH_2Cl_2$ (50 mL) was added. The solution was washed with a saturated $NaHCO_3$ solution, and the organic phase was dried on $MgSO_4$. The crude product, obtained after evaporation of the solvent (*without* heating the bath), was purified on a short column (silica gel, $CHCl_3$), and led to a white solid (960 mg, 99%). M.p. 140 °C; $^1H$ NMR ([D6]acetone): $\delta = 10.16$ (s, 2H, CHO), 8.43 (t, 1H, $^3J$(H,H) = 1.5 Hz, Ph), 8.28 (d, 2H, $^3J$(H,H) = 1.5 Hz, Ph), 3.96 (s, 1H, C≡CH), $^{13}C$ NMR ([D6]acetone): $\delta = 191.1$ (CHO), 139.1, 138.2, 130.3, 125.3 (Ph), 82.1 (-C≡C-), 81.0 (-C≡C-), IR (KBr): $\tilde{\nu} = 2115$ (C≡C), 1696 $cm^{-1}$ (CHO); elemental analysis (%) calcd for $C_{10}H_6O_2$ (158.1): C 75.94, H 3.82, O 20.23; found: C 76.10, H 3.71, O 20.38.

**1,3-Bis(1,3-dihydroxy-4,4,5,5-tetramethylimidazolin-2-yl)-5-ethynylbenzene (6)**: The same procedure as described for compound **4**, starting from **3** (995 mg, 6.3 mmol), 2,3-bis(hydroxylamino)-2,3-dimethylbutane (1.87 g, 12.63 mmol) in MeOH (35 mL) was used. A white powder was isolated (2.22 g, 85%). $^1H$ NMR ([D6]acetone): $\delta = 7.66$ (t, 1H, $^3J$(H,H) = 1.5 Hz, Ph), 7.55 (d, 2H, $^3J$(H,H) = 1.5 Hz, Ph), 7.10 (s, 4H, OH), 4.68 (s, 2H, CH imid), 3.29 (s, 1H, C≡CH), 1.17 (s, 6H, $CH_3$), 1.08 (s, 6H, $CH_3$); $^{13}C$ NMR ([D6]DMSO): $\delta = 142.1$, 130.3, 129.1, 120.1 (Ph), 90.0 (-CH imid.), 84.1 (-C≡C-), 79.3 (-C≡C-), 66.1 ($C_{quat}$ imid.), 24.0 ($CH_3$), 17.1 ($CH_3$); IR (KBr): $\tilde{\nu} = 2107$ (C≡C), 3440 $cm^{-1}$ (OH); elemental analysis calcd (%) for $C_{22}H_{34}N_4O_4$ (418.5): C 63.13, H 8.19, N 13.39; found: C 63.45, H 8.05, N 13.75.

**1,3-Bis(1-oxyl-3-oxo-4,4,5,5-tetramethylimidazolin-2-yl)-5-ethynylbenzene (diNN-tr)**: The same procedure as described for compound **diNN-H** using compound **6** (205 mg, 0.49 mmol) and $NaIO_4$ (220 mg, 1.03 mmol) in $CH_2Cl_2$/$H_2O$1:1 (40 mL) was used. After purification by chromatography (silica gel, ethyl acetate/$CH_2Cl_2$ 10:90), the product was recrystallised in $CH_2Cl_2$/hexane to afford dark blue needles (155 mg, 77%). IR (KBr): $\tilde{\nu} =$ 2103 (C≡C), 1360 $cm^{-1}$ (N–O); UV/Vis $\lambda_{max}$ ($\varepsilon$) = 259 (35 280), 369 (20 630), 589 (791), 617 nm (753 $M^{-1}cm^{-1}$); elemental analysis (%) calcd for $C_{22}H_{28}N_4O_4$ (412.5): C 64.06, H 6.84, N 13.58; found: C 63.99, H 6.82, N 13.60; FAB+ (*m*-NBA): 412.0 $[M]^+$, 397.0 $[M-O]^+$, 381.0 $[M-2O]^+$, 365.1 $[M-3O]^+$, 349.1 $[M-4O]^+$, 282.0; $N_S = 2.1$ spins per molecule.

**1,3-Bis(1-oxyl-4,4,5,5-tetramethylimidazolin-2-yl)-5-ethynylbenzene (diIN-tr)**: The same procedure as described for compound **diIN-H** using **diNN-tr** (125 mg, 0.30 mmol) and $NaNO_2$ (206 mg, 3.0 mmol) was used. After purification by chromatography (silica gel, ethyl acetate/$CH_2Cl_2$ 5:95), the product was recrystallised in $CH_2Cl_2$/hexane to afford red needles (77 mg, 67%). M.p. 174 °C; IR: $\tilde{\nu} = 2102$ (C≡C), 1370 (N–O), 1542 $cm^{-1}$ (C=N); UV/Vis: $\lambda_{max}$ ($\varepsilon$) = 301 (5960), 445 nm (789 $M^{-1}cm^{-1}$); elemental analysis (%) calcd for $C_{22}H_{28}N_4O_2$ (380.5): C 69.45, H 7.42, N 14.72; found: C 69.40, H 7.46, N 14.79; FAB+ (m-NBA): 382.0 $[M+H]^+$, 366.0, 350.0 $[M-2O]^+$; $N_S = 1.85$ spins per molecule.

**1-(1-Oxyl-4,4,5,5-tetramethylimidazolin-2-yl)-3-(1-oxyl-3-oxo-4,4,5,5-tetramethylimidazolin-2-yl)-5-ethynylbenzene (INNN-tr)**: The same procedure as described for compound **INNN-H** using **diNN-tr** (100 mg, 0.24 mmol) and $NaNO_2$ (33 mg, 0.48 mmol) as starting materials was used. After purification by chromatography (silica gel, ethyl acetate/$CH_2Cl_2$ 2:98), the product was recrystallised in $CH_2Cl_2$/hexane to afford a grey microcrystalline powder (32 mg, 34%). M.p. 188 °C; IR (KBr): $\tilde{\nu} = 2115$ (C≡C), 1364 (N–O), 1553 $cm^{-1}$ (C=N); UV/Vis: $\lambda_{max}$ ($\varepsilon$): 369 (13 680), 446 (614), 587 (512), 618 nm (469 $M^{-1}cm^{-1}$); elemental analysis (%) calcd for $C_{22}H_{28}N_4O_3$ (396.5): C 66.65, H 7.12, N 14.13; found: C 66.84, H 7.06, N 13.98; FAB+ (*m*-NBA): 397.0 $[M]^+$, 382.0 $[M-O]^+$, 366.0 $[M-2O]^+$, 349.0 $[M-3O]^+$, 283.0 $[M-4O]^+$, 267.0; $N_S = 1.9$ spins per molecule.

## Acknowledgements

This work was supported by a grant from the French government (L. Catala, PhD Thesis) and an EC COST Chemistry Action D4/0008/93. We thank Mr. Maxime Bernard (ICS, Strasbourg) for technical assistance in the EPR measurements, and Mr. Richard Poinsot (IPCMS, Strasbourg) for most of the magnetic susceptibility measurements. We also thank Prof. Elie Belorizky (Université de Grenoble) and Dr. Marc Drillon (IPCMS, Strasbourg) for providing us with the four-spins models.

[1] For a general review of the state-of-art in the field, see: *Magnetic Properties of Organic Materials* (Ed.: P. M. Lahti), Marcel Dekker, New York, **1999**, and references therein.

[2] M. Kinoshita, P. Turek, M. Tamura, K. Nozawa, D. Shiomi, Y. Nakazawa, M. Ishikawa, M. Takahashi, K. Awaga, T. Inabe, Y. Maruyama, *Chem. Lett.* **1991**, 1225; M. Tamura, Y. Nakazawa, D. Shiomi, K. Nozawa, Y. Hosokoshi, M. Ishikawa, M. Takahashi, M. Kinoshita, *Chem. Phys. Lett.* **1991**, *186*, 401.

[3] Some recent examples of the use of $\alpha$-nitronyl nitroxides: a) Y. Pei, O. Kahn, M. A. Abersold, L. Ouahab, F. Le Berre, L. Pardi, J.-L. Tholence, *Adv. Mater.* **1994**, *6*, 681; b) T. Sugawara, M. Matsushita, A. Izuoka, N. Wada, N. Takeda, M. Ishikawa, *J. Chem. Soc. Chem. Commun.* **1994**, 1723; c) K. Awaga, A. Yamaguchi, T. Okuno, T. Inabe, T. Nakamura, M. Matsumoto, Y. Maruyama, *J. Mater. Chem.* **1994**, *4*, 1377; d) A. Canneschi, F. Ferraro, D. Gatteschi, A. Le Lirzin, M. A. Novak, E. Rentschler, R. Sessoli, *Adv. Mater.* **1995**, *7*, 476; e) J. Cirujeda, E. Hernandez-Gasio, C. Rovira, J.-L. Stanger, P. Turek, J. Veciana, *J. Mater. Chem.* **1995**, *5*, 243; f) T. Mitsumori, K. Inoue, N. Koga, H. Iwamura, *J. Am. Chem. Soc.* **1995**, *117*, 2467; g) A. Lang, Y. Pei, L. Ouahab, O. Kahn, *Adv. Mater.* **1996**, *8*, 60; h) M. Matsushita, A. Izuoka, T. Sugawara, T. Kobayashi, N. Wada, N. Takeda, M. Ishikawa, *J. Am. Chem. Soc.* **1997**, *119*, 4369; i) N. Yoshioka, M. Irisawa, Y. Mochizuki, T. Kano, H. Inoue, S. Oliba, *Chem. Lett.* **1997**, 251; j) R. Akabane, M. Tanaka, K. Matsuo, N. Koga, *J. Org. Chem.* **1997**, *62*, 8854; k) S. Nakatsuji, H. Anzai, *J. Mater. Chem.* **1997**, *7*, 2161; l) S. Nakatsuji, M. Saiga, N. Hage, A. Naito, T. Hirayana, M. Nakagawa, Y. Oda, H. Anzai, K. Suzuki, T. Enoki, M. Mito, K. Takeda, *New J. Chem.* **1998**, *22*, 275; m) M. Tanaka, K. Matsuda, T. Itoh, H. Iwamura, *J. Am. Chem. Soc.* **1998**, *120*, 7168; n) T. Otsuka, T. Okuno, K. Awaga, T. Inabe, *J. Mater. Chem.* **1998**, *8*, 1157.

[4] a) H. C. Longuet-Higgins, *J. Chem. Phys.* **1950**, *18*, 265; b) W. T. Borden, E. R. Davidson, *J. Am. Chem. Soc.* **1977**, *99*, 4587; c) A. A. Ovchinnikov, *Theor. Chim. Acta* **1978**, *47*, 297; d) D. J. Klein, C. J. Nelin, S. Alexander, F. A. Matsen, *J. Chem. Phys.* **1982**, *77*, 3101; e) T. Matsumoto, T. Ishida, N. Koga, H. Iwamura, *J. Am. Chem. Soc.* **1992**, *114*, 9952; f) M. Dvolaitzky, R. Chiarelli, A. Rassat, *Angew. Chem.* **1992**, *104*, 220; *Angew. Chem. Int. Ed. Engl.* **1992**, *31*, 180.

[5] a) S. K. Silverman, D. Dougherty, *J. Phys. Chem.* **1993**, *97*, 13273; b) F. Kanno, K. Inoue, N. Koga, H. Iwamura, *J. Am. Chem. Soc.* **1993**, *115*, 847; c) N. Yoshioka, P. M. Lahti, K. Takashi, Y. Kuzumaki, E. Tsuchida, H. Nishide, *J. Org. Chem.* **1994**, *59*, 4272; d) W. T. Borden, H. Iwamura, J. A. Berson, *Acc. Chem. Res.* **1994**, *27*, 109; e) J. Fujita, M. Tanka, H. Suemune, N. Koga, K. Matsuda, H. Iwamura, *J. Am. Chem. Soc.* **1996**, *118*, 9347; f) D. Schultz, A. K. Boal, G. T. Farmer, *J. Am. Chem. Soc.* **1997**, *119*, 3846.

[6] Some examples of studies of intramolecular magnetic interactions: a) C. Ling, M. Minato, P. M. Lahti, H. Willingen, *J. Am. Chem. Soc.* **1992**, *114*, 9959; b) T. Mitsumori, K. Inoue, N. Koga, H. Iwamura, *J. Am. Chem. Soc.* **1995**, *117*, 2467; c) T. Kaneko, S. Toriu, E. Tsuchida, H. Nishide, D. Yamaki, Y. Maruta, K. Yamagushi, *Chem. Lett.* **1995**, 421; d) A. P. West, S. K. Silverman, D. A. Dougherty, *J. Am. Chem. Soc.* **1996**, *118*, 1452; e) H. Nishide, T. Kaneko, T. Nii, K. Katoh, E. Tsuchida, P. M. Lahti, *J. Am. Chem. Soc.* **1996**, *118*, 9695; f) H. Nishide, Y. Hozumi, T. Nii, E. Tsuchida, *Macromolecules* **1997**, *30*, 3986; g) M. Minato, P. M. Lahti, *J. Am. Chem. Soc.* **1997**, *119*, 2187.

[7] a) G. R. Desiraju, *Acc. Chem. Res.* **1991**, *24*, 290; b) G. R. Desiraju, *Angew. Chem.* **1995**, *107*, 2541; *Angew. Chem. Int. Ed. Engl.* **1995**, *34*, 2311.

[8] Examples of the use of hydrogen bonds in nitronyl nitroxide-based materials: a) E. Hernandez, M. Mas, E. Molins, C. Rovira, J. Veciana, *Angew. Chem.* **1993**, *105*, 919; *Angew. Chem. Int. Ed. Engl.* **1993**, *32*, 882; b) J. Cirujeda, L. E. Ochando, J. M. Amigo, C. Rovira, J. Ruis, J. Veciana, *Angew. Chem.* **1995**, *107*, 99; *Angew. Chem. Int. Ed. Engl.* **1995**, *34*, 55; c) J. Cirujeda, M. Mas, E. Molins, F. Lanfranc de Panthou, J. Laugier, J. G. Park, C. Paulsen, P. Rey, C. Rovira, J. Veciana, *J. Chem. Soc. Chem. Commun.* **1995**, 709; d) F. M. Romero, R. Ziessel, A. De Cian, J. Fischer, P. Turek, *New J. Chem.* **1996**, *20*, 919; e) J. Veciana, J. Cirujeda, C. Rovira, E. Molins, J. J. Novoa, *J. Phys. Fr.* **1996**, 1967; f) F. M. Romero, R. Ziessel, M. Drillon, J.-L. Tholence, C. Paulsen, N. Kyritsakas, J. Fischer, *J. Adv. Mater.* **1996**, *8*, 826; g) M. Matsuchida, A. Izuoka, T. Sugawara, T. Kobayashi, N. Wada, N. Takeda, M. Ishikawa, *J. Am. Chem. Soc.* **1997**, *119*, 4369; h) T. Asita, K. Kobayashi, *Adv. Mater.* **1997**, *9*, 346; i) C. Stroh, F. M. Romero, N. Kyritsakas, L. Catala, P. Turek, R. Ziessel, *J. Mater. Chem.* **1999**, *9*, 875; j) F. M. Romero, R. Ziessel, M. Bonnet, Y. Pontillon, E. Ressouche, J. Schweitzer, B. Delley, A. Grand, C. Paulsen, *J. Am. Chem. Soc.* **2000**, *122*, 1298.

[9] a) M. Deumal, J. Cirujeda, J. Veciana, J. J. Novoa, *Chem. Phys. Lett.* **1997**, *265*, 190; b) M. Deumal, J. Cirujeda, J. Veciana, J. J. Novoa, *Adv. Mater.* **1998**, *10*, 1461; c) M. Deumal, J. Cirujeda, J. Veciana, J. J. Novoa, *Chem. Eur. J.* **1999**, *5*, 1631.

[10] a) P. Wautelet, A. Bieber, P. Turek, J. Le Moigne, J.-J. André, *Mol. Cryst. Liq. Cryst.* **1997**, *305*, 55; b) P. Wautelet, *PhD Thesis*, University Louis Pasteur, Strasbourg, France, **1996**.

[11] a) D. Shiomi, M. Tamura, H. Sawa, R. Kato, M. Kinoshita, *J. Phys. Soc. Jpn.* **1993**, *62*, 289; b) A. Caneschi, P. Chiesi, L. David, D. Gatteschi, R. Sessoli, *Inorg. Chem.* **1993**, *32*, 1445; c) A. Izuoka, M. Fukada, T. Sugawara, *Mol. Cryst. Liq. Cryst.* **1993**, *232*, 103.

[12] 5-Bromoisophthalic acid was obtained and reduced to the corresponding diol as described in: a) J. A. Wytko, J. Weiss, *Tetrahedron Lett.* **1991**, *32*, 7261. The corresponding aldehyde was obtained by oxidation of the diol as described in: b) K. Netzke, G. Snatzke, *Chem. Ber.* **1989**, *122*, 1365.

[13] S. Takahashi, Y. Kuroyama, K. Sonogashira, N. Hagihara, *Synthesis* **1980**, 627.

[14] a) R. Sayre, *J. Am. Chem. Soc.* **1955**, *77*, 6689; b) M. Lamchen, T. W. Mittag, *J. Chem. Soc.* **1966**, 2300.

[15] E. F. Ullman, J. H. Osiecki, D. G. B. Boocock, R. Darcy, *J. Am. Chem. Soc.* **1972**, *94*, 7049.

[16] J. E. Wertz, J. R. Bolton, *Electron Spin Resonance, Elementary Theory and Practical Applications*, Chapman & Hall, **1986**, pp. 250–255.

[17] a) J. A. Berson, in *The Chemistry of Quinonoid Compounds, Vol. 11* (Eds.: S. Patai, Z. Rappoport), **1988**, pp. 481; b) A. Rajcah, *Chem. Rev.* **1994**, *94*, 871; c) K. Matsuda, H. Iwamura, *J. Chem. Soc. Perkin Trans. 2* **1998**, 102.

[18] B. Bleaney, K. D. Bowers, *Proc. R. Soc. London Ser. A* **1952**, *214*, 451.

[19] a) L. Noodleman, *J. Chem. Phys.* **1981**, *74*, 5737; b) L. Noodleman, E. Davidson, *Chem. Phys.* **1986**, *109*, 131; c) L. Noodleman, D. A. Case, *Adv. Inorg. Chem.* **1992**, *38*, 423.

[20] *GAUSSIAN-98*, *Rev A7*, M. J. Frisch, G. W. Trucks, H. B. Schlegel, G. E. Scuseria, M. A. Robb, J. R. Cheeseman, V. G. Zakrzewski, J. A. Jr. Montgomery, R. E. Stratmann, J. C. Burant, S. Dapprich, J. M. Millam, A. D. Daniels, K. N. Kudin, M. C. Strain, O. Farkas, J. Tomasi, V. Barone, M. Cossi, R. Cammi, B. Mennucci, C. Pomelli, C. Adamo, S. Clifford, J. Ochterski, G. A. Petersson, P. Y. Ayala, Q. Cui, K. Morokuma, D. K. Malick, A. D. Rabuck, K. Raghavachari, J. B. Foresman, J. Cioslowski, J. V. Ortiz, A. G. Baboul, B. B. Stefanov, G. Liu, A. Liashenko, P. Piskorz, I. Komaromi, R. Gomperts, R. L. Martin, D. J. Fox, T. Keith, M. A. Al-Laham, C. Y. Peng, A. Nanayakkara, C. Gonzalez, M. Challacombe, P. M. W. Gill, B. Johnson, W. Chen, M. W. Wong, J. L. Andres, C. Gonzalez, M. Head-Gordon, E. S. Replogle, J. A. Pople, Gaussian, Inc., Pittsburgh PA, **1998**.

[21] a) Broken symmetry has been used to describe with reliability inorganic dimers: See, for example: a) J. Cano, P. Alemany, S. Alvarez, M. Verdaguer, E. Ruiz, *Chem. Eur. J.* **1998**, *4*, 476; b) E. Ruiz, J. Cano, S. Alvarez, P. Alemany, *J. Am. Chem. Soc.* **1998**, *120*, 11122; c) E. Ruiz, J. Cano, S. Alvarez, P. Alemany, *J. Comput. Chem.* **1999**, *20*, 1391.

[22] See the extensive and detailed discussion in the work of: J. Gräfenstein, A. M. Hjerpe, E. Kraka, D. Cramer, *J. Phys. Chem. A* **2000**, *104*, 1758. See also: J. Pople, P. M. Gill, N. C. Handy, *Int. J. Quantum Chem.* **1995**, *56*, 303.

[23] L. Fang, M. S. Shu, D. A. Hrovat, W. T. Borden, *J. Am. Chem. Soc.* **1995**, *117*, 6727.

[24] T. Ishida, H. Iwamura, *J. Am. Chem. Soc.* **1991**, *113*, 4238.

[25] H. M. McConnell, *J. Chem. Phys.* **1963**, *39*, 1910.

[26] M. Deumal, J. J. Novoa, M. J. Bearpark, P. Celani, M. Olivucci, M. A. Robb, *J. Phys. Chem. A* **1998**, *102*, 8404.

[27] D. Shiomi, M. Tamura, H. A. Katori, T. Goto, A. Hayashi, Y. Ueda, R. Kato, M. Kinoshita, *J. Mater. Chem.* **1994**, *4*, 915.

[28] E. Belorizky, *J. Phys. I Fr.* **1993**, *3*, 423.

[29] K. Yamaguchi, in *Magnetic Properties of Organic Materials* (Ed.: P. M. Lahti), Marcel Dekker, New York, Chapter 20, p. 403, **1999**.

[30] P. Turek, *Magnetic Properties of Organic Materials* (Ed.: P. M. Lahti), Marcel Dekker, New York, Chapter 24, p. 491, **1999**.

[31] The full study of the anisotropic EPR response is reported in the Supporting Information (see Figures S3–S6).

[32] a) F. Lanfranc de Panthou, D. Luneau, J. Laugier, P. Rey, *J. Am. Chem. Soc.* **1993**, *115*, 9095; b) N. Yoshioka, M. Irisawa, Y. Mochizuki, T. Kato, H. Inoue, S. Ohba, *Chem. Lett.* **1997**, 251.

[33] For details of the probabilities of each model, see the Supporting Information.

[34] A. Zheludev, V. Barone, M. Bonnet, B. Delley, A. Grand, E. Ressouche, P. Rey, R. Subra, J. Schweizer, *J. Am. Chem. Soc.* **1994**, *116*, 2019.

[35] J. J. Borras-Almenar, E. Coronado, J. Curely, R. Georges, J. C. Guianduzzo, *Inorg. Chem.* **1994**, *33*, 5171.


Received: November 24, 2000 [F2892]